AUG 13

GRADUATE AERONAUTICAL LABORATORIES
CALIFORNIA INSTITUTE OF TECHNOLOGY

Mixing, chemical reactions, and combustion in subsonic and supersonic turbulent flows

Paul E. Dimotakis and Anthony Leonard

Air Force Office of Scientific Research
Grant No. F49620–98–1–0052 Final Scientific Report

28 February 2001

DISTRIBUTION STATEMENT A
Approved for Public Release
Distribution Unlimited

20011003 050

Firestone Flight Sciences Laboratory

Guggenheim Aeronautical Laboratory

Karman Laboratory of Fluid Mechanics and Jet Propulsion

Pasadena

REPORT DOCUMENTATION PAGE

AFRL-SR-BL-TR-01-

0477

Public reporting burden for this collection of information is estimated to average 1 hour per response, including the time for reviewing instructi data needed, and completing and reviewing this collection of information. Send comments regarding this burden estimate or any other aspec this burden to Department of Defense, Washington Headquarters Services, Directorate for Information Operations and Reports (0704-0188), 4302. Respondents should be aware that notwithstanding any other provision of law, no person shall be subject to any penalty for failing to c valid OMB control number. **PLEASE DO NOT RETURN YOUR FORM TO THE ABOVE ADDRESS.**

1. REPORT DATE *(DD-MM-YYYY)*	2. REPORT TYPE	3. DATES COVERED *(From - To)*
28-02-2001	Final Technical Report	1-10-1997 to 30-11-2000

4. TITLE AND SUBTITLE
Mixing, chemical reactions, and combustion in subsonic and supersonic turbulent flows

5a. CONTRACT NUMBER

5b. GRANT NUMBER
F49620-98-1-0052

5c. PROGRAM ELEMENT NUMBER
61102F

6. AUTHOR(S)
Paul E. Dimotakis and Anthony Leonard

5d. PROJECT NUMBER
2308

5e. TASK NUMBER
BS/BV

5f. WORK UNIT NUMBER

7. PERFORMING ORGANIZATION NAME(S) AND ADDRESS(ES)

Paul E. Dimotakis
Mail Code 301-46, Aeronautics
Calif. Inst. Of Technology
Pasadena, CA 91125

8. PERFORMING ORGANIZATION REPORT NUMBER

9. SPONSORING / MONITORING AGENCY NAME(S) AND ADDRESS(ES)

AFOSR/NA
801 N. Randolph St. Room 732
Arlington, VA 22203-1977

10. SPONSOR/MONITOR'S ACRONYM(S)

11. SPONSOR/MONITOR'S REPORT NUMBER(S)

12. DISTRIBUTION / AVAILABILITY STATEMENT

Approved for public release; distribution is unlimited

13. SUPPLEMENTARY NOTES

14. ABSTRACT

Research conducted under sponsorship of this grant focused on fundamental investigations of mixing, chemical-reaction, and combustion processes, in turbulent, subsonic, and supersonic flows. Research on hydrocarbon-combustion extended previous work highlighting deficiencies in existing chemical-kinetics models for ethylene combustion. Experiments in the 2- and 3-D structure and mixing of turbulent transverse jets yielded new results on isotropy and Reynolds number effects. Work in high-speed flows and subsonic-diffusers demonstrated considerable control via mass injection. Direct numerical simulations of Rayleigh-Taylor instability flows attained the highest Reynolds numbers to date yielding results on mixing and over-all growth rates. Image Correlation Velocimetry was applied to free jets and OH-tagged lines. Advances in high-performance digital-imaging systems were implemented, permitting high frame-rate and high-resolution multi-dimensional data acquisition in many of the experiments.

15. SUBJECT TERMS
Combustion, mixing, subsonic, supersonic, turbulence, hydrocarbon, transverse jets, Image Correlation Velocimetry, Rayleigh-Taylor instability, high-performance digital imaging.

16. SECURITY CLASSIFICATION OF:			17. LIMITATION OF ABSTRACT	18. NUMBER OF PAGES	19a. NAME OF RESPONSIBLE PERSON
Unclassified					Dr. Julian Tishkoff
a. REPORT	b. ABSTRACT	c. THIS PAGE	None	48	19b. TELEPHONE NUMBER *(include area code)*
Unclassified	Unclassified	Unclassified			(703) 696-8478

GRADUATE AERONAUTICAL LABORATORIES
CALIFORNIA INSTITUTE of TECHNOLOGY
Pasadena, California 91125

Mixing, chemical reactions, and combustion in subsonic and supersonic turbulent flows

Paul E. Dimotakis* and Anthony Leonard**

Air Force Office of Scientific Research
Grant No. F49620–98–1–0052

Final Scientific Report
1 October 1997 through 30 November 2000

28 February 2001

* John K. Northrop Professor of Aeronautics and Professor of Applied Physics

** Theodore von Kármán Professor of Aeronautics

Summary

Research conducted under sponsorship of this grant (F49620–98–1–0052) focused on fundamental investigations of mixing, chemical-reaction, and combustion processes, in turbulent, subsonic, and supersonic flows. Specifically, the work focused on several interrelated parts:

1. hydrocarbon-combustion kinetics and hydrocarbon-flame behavior,
2. mixing in turbulent transverse jets,
3. mixing in high-speed flows with a focus on subsonic-diffuser control,
4. Rayleigh-Taylor instability flows,
5. advances in Image Correlation Velocimetry,

and

6. the development of high-performance digital imaging systems,

with significant progress in all of these areas, as documented below.

The program was comprised of an experimental effort; an analytical, modeling, and numerical-simulation effort; and a diagnostics- and instrumentation-development effort. Part of the numerical-simulation effort was in collaboration with Lawrence Livermore National Laboratory and work at Caltech under ASCI/ASAP contract W–7405–ENG–48. Parts of the instrumentation-development effort were cofunded by AFOSR grants F49620–95–1–0199, F49620–00–1–0036, and NSF grants AST9618880 and EIA0079871000, in collaboration with Physics, Astronomy, and the Center for Advanced Computing Research (CACR) at Caltech, and the Jet Propulsion Laboratory.

1. Research description

1.1 Hydrocarbon flames and combustion in high-speed flows

1.1.1 Direct numerical simulations

Detailed numerical investigations on the ignition of low molecular weight hydrocarbons have been performed. The motivation stems from a proposed concept (*e.g.*, Edwards 1996) for future hypersonic air-breathing combustion, using practical endothermic hydrocarbon fuels. The concept pertains to flight Mach numbers in the range, $4 \leq M_\infty \leq 8$. For typical static temperatures, T_∞, in the range $250\,K \leq T_\infty \leq 300\,K$, stagnation temperatures, T_0, for a perfect gas are expected to be in the range of $1000\,K \leq T_0 \leq 4000\,K$ (Egolfopoulos, Dimotakis, & Bond 1996,Egolfopoulos & Dimotakis 2000a). Ignition and flame stability characteristics of hydrocarbons set the proposed lower limit of M_∞. The upper M_∞ limit is set by the cooling capacity of such fuels, used as endothermic fuels, *e.g.*, of kerosene-type, to cool the fuselage and the internal-flow passages. It has been estimated (Edwards 1996) that fuel temperatures can be as high as $1050\,K$, and for such temperatures, thermodynamics indicate that fuel molecules are thermally decomposed, through thermal cracking. For fuel temperatures, $T_{\rm fuel}$, in the range, $800\,K \leq T_{\rm fuel} \leq 1050\,K$, equilibrium calculations were performed (Egolfopoulos & Dimotakis 1998) to determine the composition of the fuel blend expected from thermal cracking of $C_{12}H_{26}$, a representative constituent of kerosene-type fuels. It was found that the composition is largely controlled by nearly equal amounts of CH_4 and C_2H_4, with smaller amounts of H_2, C_2H_2, C_2H_6, with $C_3 - C_4$ hydrocarbons also present.

The goal of this investigation was to numerically assess the ignition characteristics of such fuel blends, for conditions of relevance to proposed SCRAMJET concepts. While the pressure and temperature conditions can be determined with good accuracy, the magnitude of strain rates that will be locally encountered by the reacting layers can be only estimated from global fluid mechanics arguments to be in the range of $10^4 - 10^6 s^{-1}$ (Egolfopoulos, Dimotakis, & Bond 1996). Such strain-rate values provide guidelines in assessing the ability of the fuel blends to ignite.

Numerical simulations of laminar flame speeds were performed using the PREMIX code (Kee *et al.* 1985). Investigations of a heated-fuel jet counterflowing against a heated-air jet permitted an assessment of the effect of strain rate. The non-premixed configuration is representative of combustion in SCRAMJETS, and its numerical simulation was performed using a stagnation-flow code (Egolfopoulos & Campbell 1996), modified through the introduction of a two-point continuation allowing for the description of the entire Z-curve flame response to strain rate. Both codes were integrated with the CHEMKIN (Kee *et al.* 1989) and Transport (Kee *et al.* 1983) subroutine libraries.

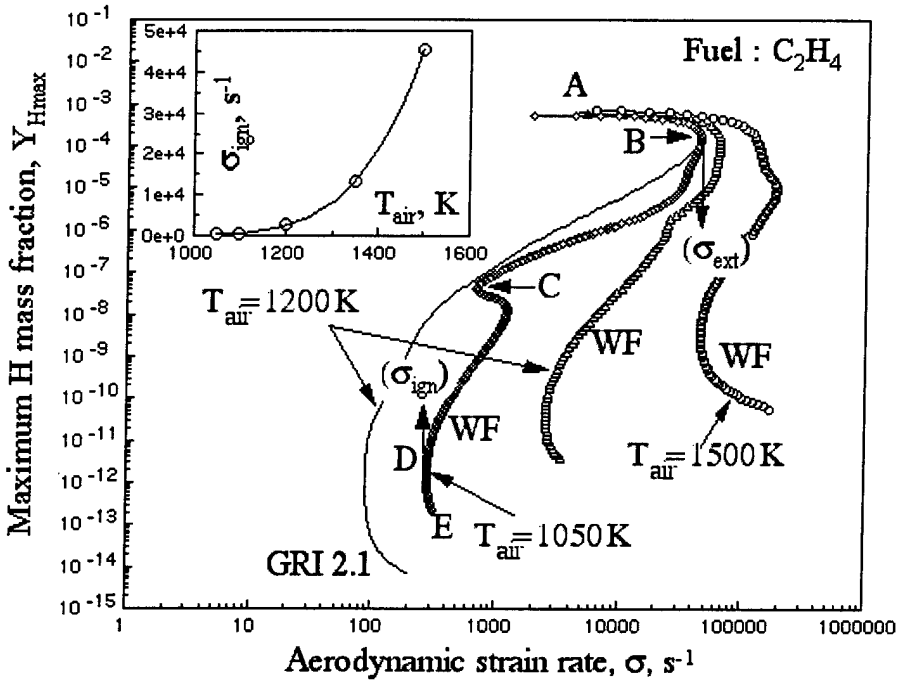

FIG. 1 Effects of T_{air} on Z-curve response of non-premixed C_2H_4/air, for $T_{\text{fuel}} = 950\,\text{K}$, using the WF and GRI 2.1 mechanisms (see text). Inset: ignition strain rate as a function of air temperature.

Z-curves for individual constituents and their blends were determined. As anticipated, the ignition propensity of C_2H_4 was found to be superior of that of CH_4, indicating the need for further focusing on ignition promotion of C_2H_4. The Z-curve response for C_2H_4/air is shown in Fig. 1, for different values of the air temperature, T_{air}. The large sensitivity of the ignition strain rate on T_{air} is apparent. An important finding of this study was also that the omission of just one species (vinyoxy-CH_2CHO) can result in substantial differences in the prediction of ignition strain

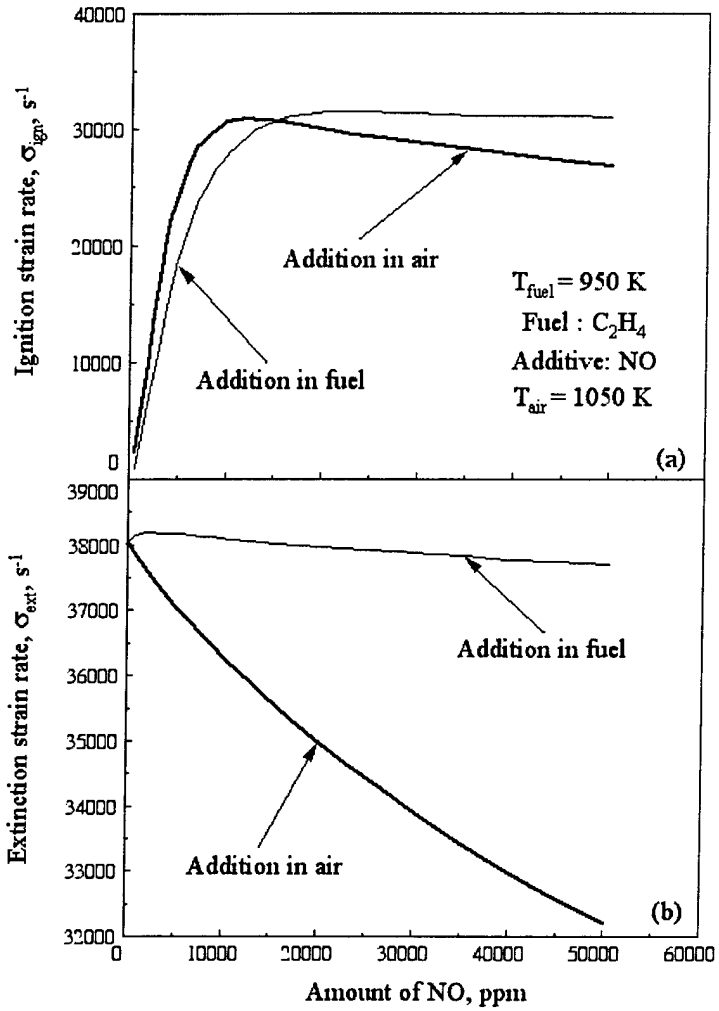

FIG. 2 Effect of NO addition on σ_{ign} and σ_{ext} of non-premixed C_2H_4/air.

rates, σ_{ign}. The GRI 2.1 (Frenklach *et al.* 1995) and the WF (Wang & Frenklach 1997) mechanisms predict values of σ_{ign} that are different by a factor of 30. The WF mechanism includes the CH_2CHO species while the GRI 2.1 does not. This study also demonstrated that the presence of H_2 and C_2H_2 does not render the blend ignitable, for the strain rates of interest. The use of additives, such as F_2 and NO was found to increase σ_{ign} noticeably, as a result of the hypergolic nature of these two chemicals.

The effect of additives such as NO, F_2, and H_2 on the ignition of C_2H_4/air, was investigated, to assess other means of enhancing ignition of C_2H_4. Small amounts of NO, F_2, and H_2 were added independently into the fuel and air streams. It was found that addition of NO results in significant increases in σ_{ign}, accompanied by a

rather moderate decrease of the extinction strain rate, σ_{ext}, when added to the air stream. See Fig. 2. Detailed analysis of the structure of the reacting layers showed that NO effectively acts as a catalyst promoting the production of OH, which in turn accelerates the fuel consumption rate and the ignition process. The Wang & Frenklach (1997, WF) kinetic scheme was used for this study.

Considering the sensitivity of the ignition process on the detailed chemical kinetics, studies of current state-of-the-art kinetics of C_2H_4 were performed (Egolfopoulos & Dimotakis 2000b). Six detailed mechanisms, compiled based on predictions of experimental results in homogeneous reactors and flames, were compared. These mechanisms are: TAN94 (Tan *et al.* 1994), GRI21 (Frenklach *et al.* 1995), WF97 (Wang & Frenklach 1997), MRN98 (Marinov *et al.* 1998, Marinov 1999),GRI30 (Bowman *et al.* 1999), and W99 (Wang *et al.* 1999).†

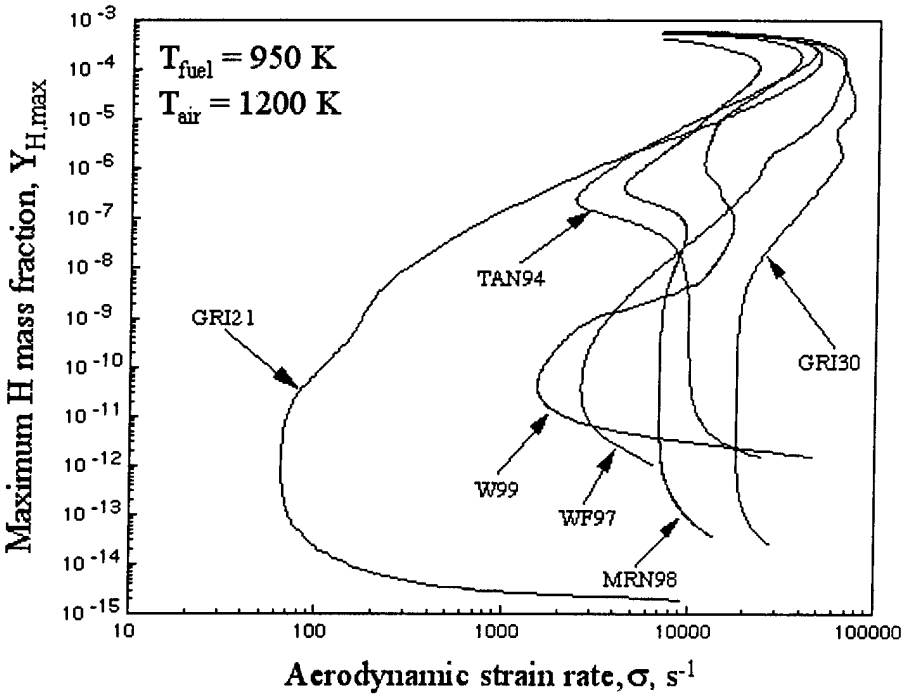

FIG. 3 Calculated Z-curve response for non-premixed C_2H_4/air.

The comparative study included simulations of both the Z-curve response and laminar flame speeds for C_2H_4/air mixtures. While laminar flame speed experimental data are available, no ignition and extinction data are presently available. Calcu-

† In the documentation of previous studies, the acronym WF was used instead of WF97.

lated Z-curves are shown in Fig. 3. The discrepancies between the various mechanisms are apparent. In particular, predicted values of σ_{ign} differ by factors as large as 300. Discrepancies of predicted values for σ_{ext} and laminar flame speeds are comparable and of the order of factors of 2.3 to 3.0. A more-complete documentation of this work and findings can be found in Egolfopoulos & Dimotakis (2000b).

These results stress the need for further kinetics studies of C_2H_4 oxidation, as well as the determination of experimental data for flame ignition, propagation, and extinction in order for the validations to be comprehensive and reliable. This part of the work is a collaboration with Prof. Fokion Egolfopoulos of the University of Southern California.

An experimental program to investigate the deficiencies and provide data to address them is described below and was begun as part of this grant and presently continues as part of AFOSR grant F49620–01–1–0006.

1.1.2 Experimental work

The primary objective of this part of the research, is to address the deficiencies in the experimental data base and, more generally, provide a significant extension of available experimental data on C_1-, C_2- and select C_3-hydrocarbon flames, at pressures in the range of $0.5\,\text{atm} < p < 12\,\text{atm}$. Such data include flame ignition, propagation and extinction in laminar premixed flames. Ignition and extinction strain-rates as well as laminar flame speeds will be determined as a function of pressure, temperature and fuel concentration. Comparison between models and such data will not only provide a validation of available kinetic models but also means of improving them. Selected diagnostics under development include, but are not limited to, chemiluminescence imaging, Particle Streak Velocimetry (Dimotakis, Debussy, & Koochesfahani 1981), as well as Planar Laser Induced Fluorescence (PLIF) for concentration profiles of radicals such as CH and OH, as discussed below.

The work as part of this grant focused on the development of the experimental diagnostics and configuration at atmospheric pressure, validation of the technique against existing data for laminar-flame properties, and design and exploratory experimentation for extension to high pressures.

The experiments entail a stagnation-type jet-flow configuration. More specifically, a premixed fuel-oxidizer (air) jet is generated through a small-diameter ($d \simeq 1\,\text{cm}$)

contoured nozzle that impinges on a solid stagnation surface. A planar, nearly-adiabatic flame is established between the exit of the nozzle and the stagnation surface at a location which is primarily a function of the imposed aerodynamic strain-rate. An illustration of the velocity field for such a methane-air flame is depicted in Fig. 4.

FIG. 4 Premixed methane-air flame in stagnation flow. Equivalence ratio: $\Phi = 0.7$. Jet-nozzle diameter: $d = 14\,\text{mm}$. Jet/plate separation distance: $L = 28\,\text{mm}$. Measured jet-nozzle exit velocity: $U_{\text{ex}} = 38\,\text{cm/s}$. Hydrodynamic strain rate: $\sigma = 22.75\,\text{s}^{-1}$.

This type of flow has been extensively documented for its quasi-one-dimensional behavior along the centerline of the flow-field (Kee *et al.* 1985). Accurate numerical descriptions of the fluid dynamics rely on this assumption. As a consequence, significant effort was expended verifying the quasi-one-dimensional nature of the flow and addressing any problems that make the flow-field diverge from it. It was demonstrated (Vagelopoulos 1999) that the radial uniformity of the axial velocity component depends on experimental parameters such as the design of the contoured nozzle and the ratio of the separation distance to the nozzle diameter (L/d), as required to avoid unfavorable radial pressure gradients.

The jet plenum and contraction section was designed to allow for accurate prediction of the boundary layer thickness and necessary velocity profile corrections at the

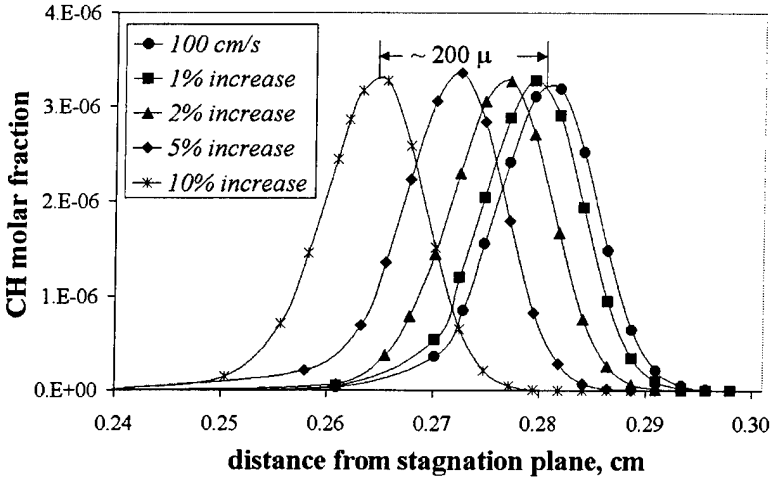

FIG. 5 Sensitivity of flame location to velocity variation. Methane-air flame: $\Phi = 1.0$. Jet nozzle diameter: $d = 1\,\text{cm}$. Jet/plate separation distance, $L = 1\,\text{cm}$. Reference jet-nozzle exit velocity: $U_{\text{ex}} = 100\,\text{cm/s}$.

the nozzle and was used in previous jet-flame work in our group (Gilbrech 1991, Gilbrech & Dimotakis 1992). The nozzle-exit velocity and its streamwise gradient is a critical boundary condition for the numerical simulations involved. Figure 5 depicts the sensitivity of the flame location (represented by the CH radical maximum concentration) to the nozzle exit velocity, as predicted by numerical simulation (Kee *et al.* 1985, Bowman *et al.* 1999).

Two independent, non-intrusive methods are used for its determination, namely a mass flow meter and a velocity determination through the Bernoulli pressure drop in the jet contraction section. Exploratory experiments verified agreement for the two methods for all conditions necessary for these experiments, with an error of the order of, or less than, 1%, *i.e.*, superior to typical diagnostic techniques employed to date. They were also consistent with the measured attendant (small) pressure rise in the high-pressure facility (Gilbrech 1991, Gilbrech & Dimotakis 1992) that will be used at elevated pressures. Finally, a second set of pitot-tube measurements for different exit velocities verified the radial dependence of the nozzle-exit velocity profile to comparable accuracy.

A third set of experiments explored the effect of L/d on flow uniformity, monitored by the developed flame curvature for small values ($L/d < 0.5$). As a general rule, values of $L/d \geq 1$ generated planar flames (Fig. 6).

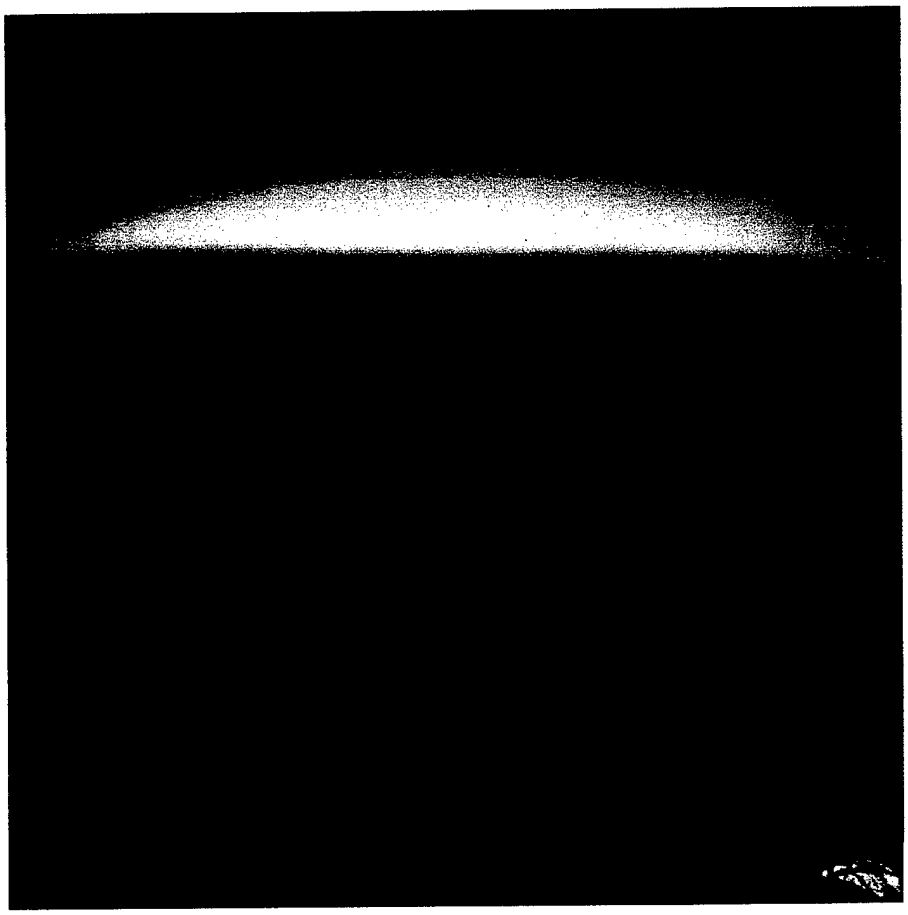

FIG. 6 Premixed methane-air flame chemiluminescence. Pressure: $p = 1\,\text{atm}$. Equivalence ratio: $\Phi = 0.8$. Jet-nozzle diameter: $d = 1\,\text{cm}$. Jet/plate separation distance: $L = 2.5\,\text{cm}$. Measured jet-nozzle exit velocity: $U_{\text{ex}} = 75\,\text{cm/s}$. Nozzle lip visible on lower right. Image resolution: 1024^2 pixels.

The stagnation plate was aerodynamically designed to minimize flame curvature and instabilities. Comparing Fig. 4, for which the jet flow was generated through a nozzle and a stagnation surface that were not optimized, with Fig. 6 the substantial reduction of flame curvature around the centerline is evident.

As noted above, another critical boundary condition is the axial velocity gradient at the exit of the nozzle. Figure 7 depicts the sensitivity of the flame location to this gradient. It was shown experimentally and numerically that, for large L/d (> 1.25), the flow has jet characteristics in the vicinity of the exit of the nozzle, with a near-zero velocity gradient.

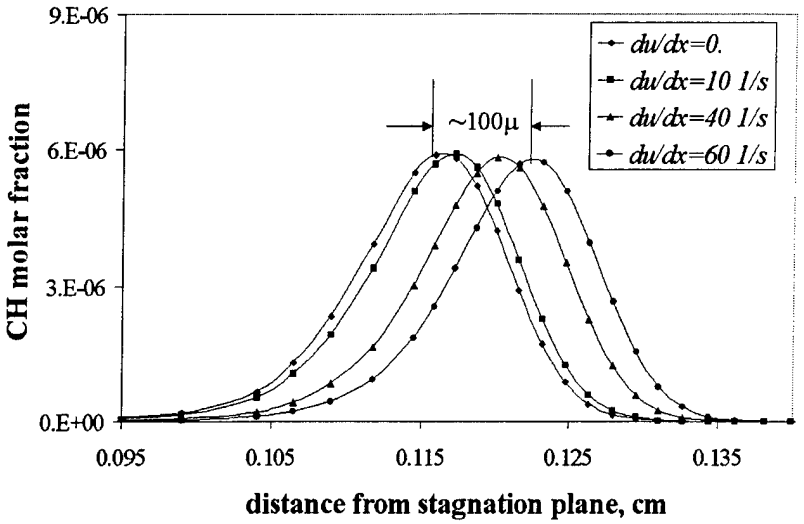

FIG. 7 Sensitivity of flame location to velocity gradient at the exit of the nozzle. Premixed methane-air flame: $\Phi = 1.0$, $p = 1\,\text{atm}$. Jet-nozzle diameter: $d = 1\,\text{cm}$. Jet-plate separation distance: $L = 1\,\text{cm}$. Numerical-simulation jet-nozzle exit velocity: $U_{\text{ex}} = 100\,\text{cm/s}$.

The axial velocity profile along the centerline was determined experimentally through LDV point measurements and compared with two-dimensional direct-numerical simulations using an axisymmetric code developed in-house by Ron Henderson. Figure 8 depicts the jet-like behavior and good agreement between the numerical-simulation and experimental data.

The lead investigator of these experiments is C. Vagelopoulos, in collaboration with J. Bergthorson. This work is presently in progress under AFOSR sponsorship (F49620–01–1–0006) with studies of methane and ethylene fuel-air mixtures, before other hydrocarbon blends are investigated.

As part of the experimental work on flames, an effort was focused to determine additional requirements these experiments will place on an imaging system. One goal is to excite CH radicals within the flame with a tunable dye laser operating in the UV, at 389 nm. CH radicals excited at 389 nm fluoresce at 432 nm and this light will be imaged.

Such imaging is difficult because the fluorescence emission is short-lived and spectrally amidst the broadband chemiluminescence emission of the flame. This represents 'noise' that cannot be removed by bandpass or other optical filters. The CH emission follows shortly after the laser excitation and lasts on the order of 10 ns.

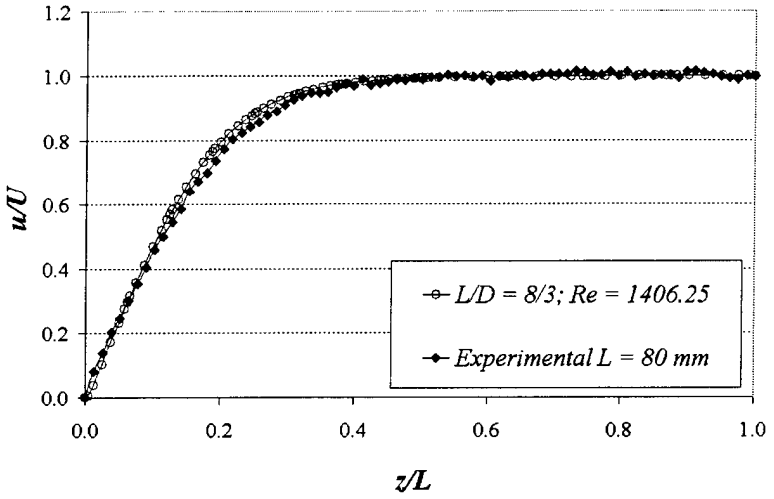

FIG. 8 Comparison of experimental (solid symbols) and numerical (open symbols) data for cold jet flow. Velocity measured with LDV diagnostics. Numerical-simulation using axisymmetric flow DNS (see text). Jet-nozzle diameter: $d = 3\,\text{cm}$. Jet/plate separation distance: $L = 8\,\text{cm}$.

When using an ungated CCD imager, chemiluminescence is recorded throughout the exposure. The short-duration fluorescence signal is negligible when compared to this integrated light from the flame and results in low signal-to-noise ratio (SNR) data. To increase SNR, gating in time is required. To 'shutter' a CCD at the relevant nanosecond time scales, an Intensified CCD (ICCD) is required. Presently available ICCD's, however, are characterized by significantly lower SNR's than our in-house digital-imaging capability, as well as offering lower framing rates (3 fps, or less). Exploratory experiments were conducted that confirmed our calculations.

Pending commercial or in-house improvements in ICCD's, with better resolution ($\geq 1024 \times 1024$ pixels) and framing rate ($\geq 10\,\text{Hz}$) diagnostics will primarily rely on high-resolution chemiluminescence imaging, in conjunction with velocity-measuring diagnostics. These provide an adequate marker for flame location. At the high anticipated pressures, these may also prove to be the preferred option. Gated, digital-imaging design studies are continuing, under F49620–01–1–0006, with an eye to improving on what is presently available.

This work is part of the Ph.D. research of J. M. Bergthorson, in collaboration with C. Vagelopoulos, and W. Pun, S. Palm, and Prof. F. Culick at Caltech.

1.2 Mixing in turbulent transverse jets

The mixing behavior of turbulent jets discharging into a crossflow, or transverse jets, was experimentally studied during this reporting period. Transverse jets are important to VTOL/STOL aerodynamics, and blade-and-endwall cooling in gas-turbine engines. The transverse jet has also been proposed as a geometry for fuel injection in high-speed airbreathing propulsion devices, such as SCRAMJETS (Mathur *et al.* 1999). The measurements of scalar fields undertaken have enabled analysis of many aspects of mixing in liquid-phase (high-Schmidt-number) transverse jets. The results of studies on Reynolds-number effects and flow dependence of turbulent mixing are discussed below.

High-resolution, high signal-to-noise-ratio images of the scalar field in transverse jets were recorded using laser-induced fluorescence (LIF) and digital-imaging techniques. For these liquid-phase experiments, rhodamine-6G was used as the fluorescent marker, and the fluid Schmidt number, $Sc \equiv \nu/\mathcal{D}$, is estimated to be $Sc \simeq 8.4 \times 10^3$ (Axelrod *et al.* 1976, Walker 1987). With appropriate calibration and normalization, these images yield quantitative measurements of the jet-fluid concentration field in two-dimensional slices. Measurements were made in streamwise (plane-of-symmetry) slices of the jet, as shown in Fig. 9. Images were also recorded in a plane normal to the freestream flow, as seen in Fig. 10. These images were recorded in the far-field of this flow, at $x/d_\mathrm{j} = 50$. The Reynolds numbers investigated were $1.0 \times 10^3 \leq Re_\mathrm{j} \leq 20 \times 10^3$, and the jet-to-freestream velocity ratio, $V_\mathrm{r} \equiv U_\mathrm{j}/U_\infty$, was $V_\mathrm{r} = 10$.

The statistics of turbulent mixing in the transverse jet are described in terms of the probability-density function (PDF) of the concentration field. PDFs define the statistics of fluctuating quantities (scalar concentration, in this case), and their moments, and are the basis for statistical approaches toward turbulent flow with chemical reactions (Pope 1985, Goldin & Menon 1997). For the transverse jet, spatial PDFs of jet-fluid concentration are computed from a sequence of 512 (1024×1024)-pixel images, yielding $\approx 5 \times 10^8$ individual (point) measurements of the scalar (jet-fluid concentration) field. Jet-fluid concentration PDFs in the far-field ($x/d_\mathrm{j} = 50$) of the jet are shown in Fig. 11 for $Re_\mathrm{j} = 1.0, 2.0, 5.0, 10$, and 20×10^3. The PDFs are monotonic-decreasing functions at low Reynolds numbers, but show a growing peak with increasing Reynolds number. At the higher Reynolds numbers, there is decreased probability for unmixed, high-concentration fluid, and a developing preference for a particular mixed-fluid concentration, C_peak. These experiments and analyses indicate more-uniform mixing (*i.e.*, better spatial homogenization)

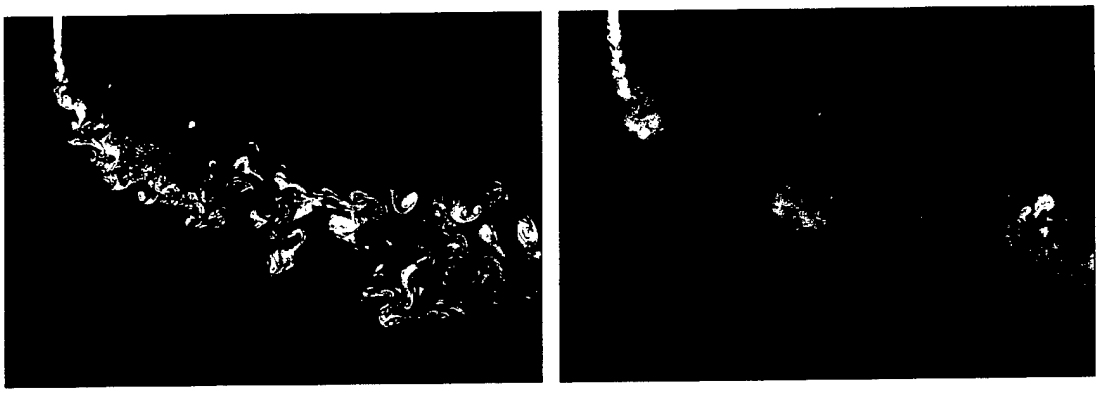

FIG. 9 Laser-induced fluorescence image data in a liquid-phase transverse jet. Streamwise (plane-of-symmetry) slice of jet for $V_r = 10$. Image intensity scaled by $x^{1/2}$ (for display purposes only) to compensate for downstream decay. Left: $Re_j = 1.0 \times 10^3$. Right: $Re_j = 10 \times 10^3$.

FIG. 10 Jet-fluid concentration in a transverse slice of jet at downstream location $x/d_j = 50$ for $V_r \simeq 10.1$. Left: $Re_j = 1.0 \times 10^3$. Right: $Re_j = 10 \times 10^3$

with increasing Reynolds number, in the range $1.0 \times 10^3 \leq Re_j \leq 20 \times 10^3$.

Comparison of the transverse-jet PDF with the PDF of ordinary turbulent jets reveals flow-dependent differences in turbulent mixing. Previous work in the group focused on the mixing behavior of liquid-phase, axisymmetric, turbulent jets discharging into a quiescent reservoir (Catrakis & Dimotakis 1996). The PDFs of these

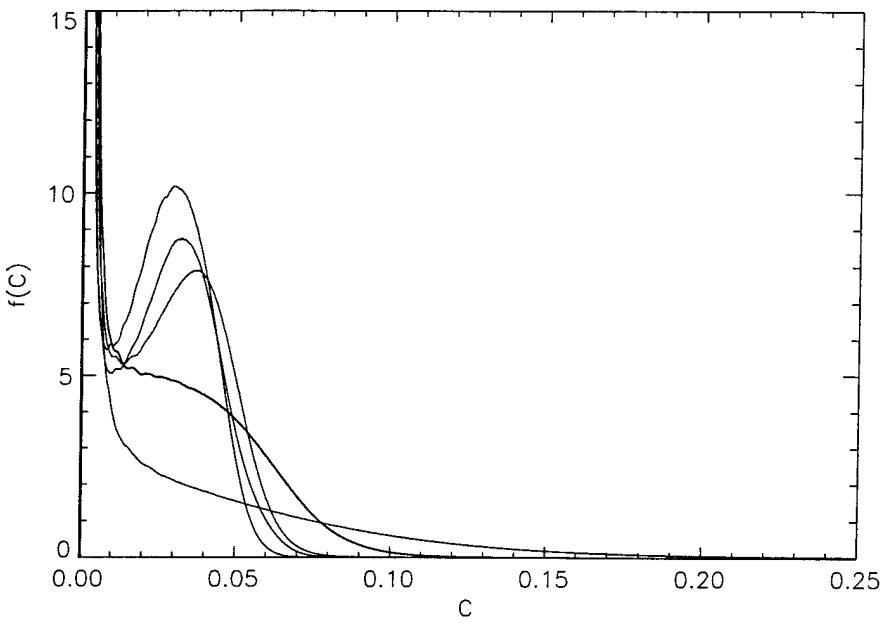

FIG. 11 Transverse-jet PDFs at $x/d_j = 50$. Concentrations normalized by plenum-exit concentration, $C = c/c_0$. Increasingly peaked PDFs at $C \simeq 0.04$ with increasing Reynolds number for $Re_j = 1.0, 2.0, 5.0, 10$, and 20×10^3.

turbulent jets, plotted in Fig. 12, show decreasing peaks with increasing Reynolds number: the "valleys" fill in, and the PDFs tend toward monotonic-decreasing functions with increasing Reynolds number. This is substantially different from the PDFs of transverse jets, which show growing peaks with increasing Reynolds number. Turbulent mixing is found to be non-universal (flow-dependent), based on the difference between transverse jets, and ordinary turbulent jets.

Two-dimensional image measurements of the scalar field, recorded in LIF images like those shown in Fig. 10, enable field measurements of scalar differences. Scalar differences,

$$\Delta_{\mathbf{r}} C \equiv C(\mathbf{x}+\mathbf{r},t) - C(\mathbf{x},t) \ , \tag{1}$$

also known as scalar increments, are differences between simultaneous measurements of the scalar field at two points separated by a distance $\mathbf{r}$. The statistics of scalar increments are important in turbulence theory (*e.g.*, scalar structure functions), and have been studied with hot-wire measurements in a variety of flows (Antonia *et al.* 1984, Ching 1991, Mydlarski & Warhaft 1998). Field measurements (rather than point measurements) of scalar increments are made by spatially shifting the measured concentration fields, and subtracting from unshifted images. Examples of two-dimensional scalar difference fields for horizontal shifts of 2 pixels, and 16 pixels, are shown in Fig. 13.

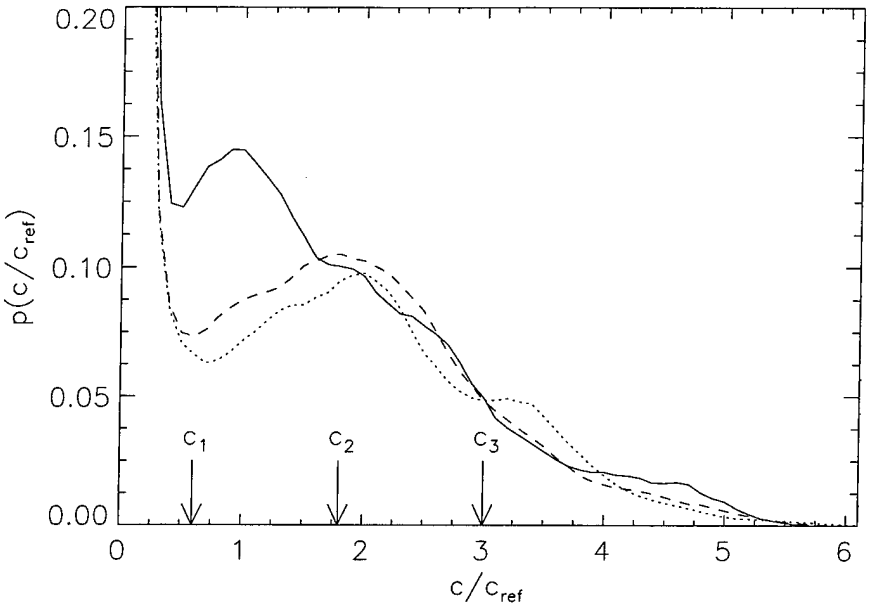

FIG. 12 Jet-in-quiescent-reservoir PDFs. Lines of increasing solidity denoting increasing $Re_j = 4.5 \times 10^3$, 9×10^3, and 18×10^3 (Catrakis & Dimotakis 1996, Fig. 8).

FIG. 13 Two-dimensional scalar-difference field. Left: Horizontal increment of 2 pixels. Right: Horizontal increment of 16 pixels.

PDFs of scalar increments are computed from normalized histograms of the scalar-difference images. The PDFs of scalar increments at $x/dj = 50$ for a variety of separation distances are shown in Fig. 14. At a jet Reynolds number of $Re_j =$

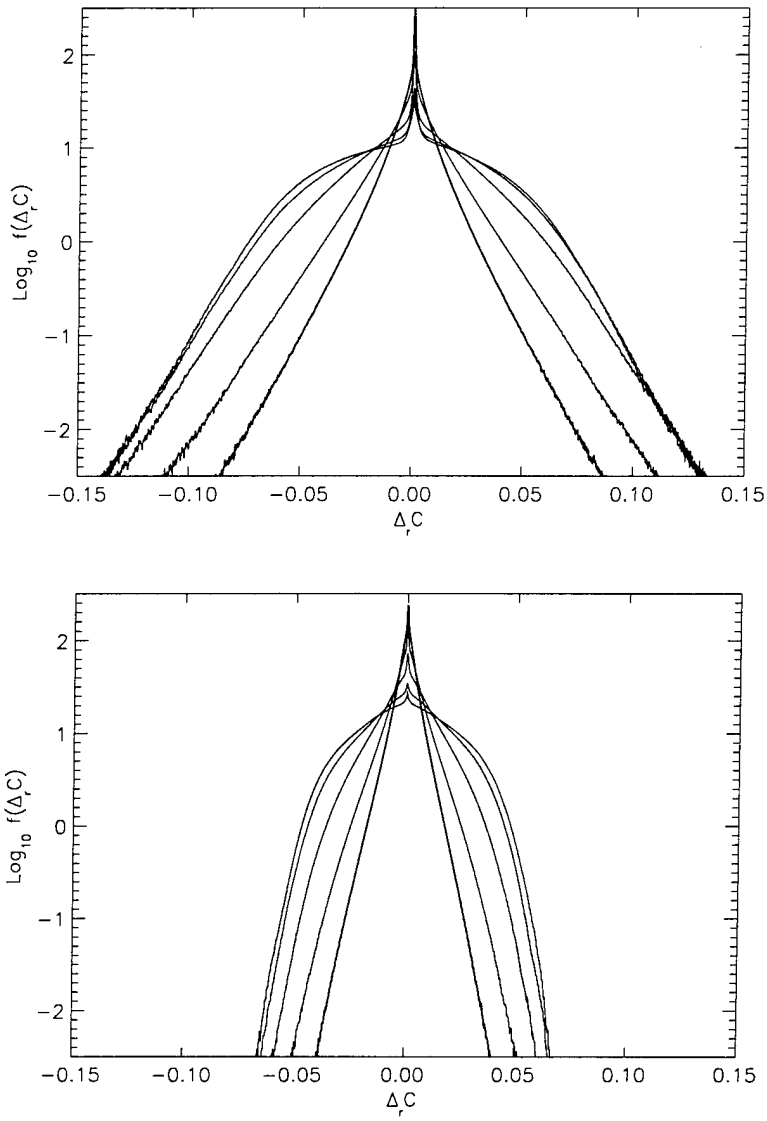

FIG. 14 PDF of scalar increments at $x/d_j = 50$ for horizontal separations of 2, 4, 16, 64, and 128 pixels. Innermost, triangular PDF is for smallest separation distance, while outermost, broad PDF is for largest separation. For comparison, the scalar diffusion scales for the $Re_j = 2.0 \times 10^3$ and 20×10^3 jets are 3 and 0.5 pixels, respectively. Top: $Re_j = 2.0 \times 10^3$. Bottom: $Re_j = 20 \times 10^3$.

20×10^3, the PDF shows exponential tails for small separations ($r = 2$ and 4 pixels). As the separation distances increase, the tails of the PDFs decay faster than an exponential. Others have reported Gaussian PDFs for large separation distances (*e.g.*, Ching 1991). At lower Reynolds numbers, $Re_j = 2.0 \times 10^3$, the PDFs are wider, indicating less mixing (poorer spatial homogenization). The PDFs for small separations are stretched exponential, and the tails of the PDFs once again decay

faster than an exponential for large separation distance. These results are consistent with those of investigations in grid turbulence, Rayleigh-Benard convection, and other flows.

This work is part of the Ph.D. research of Jerry Shan. A presentation of these results was made at the recent APS meeting of the Division of Fluid Dynamics (Shan & Dimotakis 2000). A more complete documentation is available in Shan (2001) and Shan & Dimotakis (2001).

1.3 Mixing in high-speed flows

High-speed internal flows are particularly sensitive to flow geometry as well as skin-friction effects. Traditional approaches to addressing the difficulties that ensue rely on variable geometry, with high attendant penalties in weight and complexity. The part of the work addressing high-speed mixing focused on applications of a flow field, similar to that anticipated in supersonic/hypersonic propulsors, shown in Figs. 15 and 16. During the course of this grant, the subsonic behavior of such flows was investigated. This study has important implications in the control of diffuser performance through aerodynamic means.

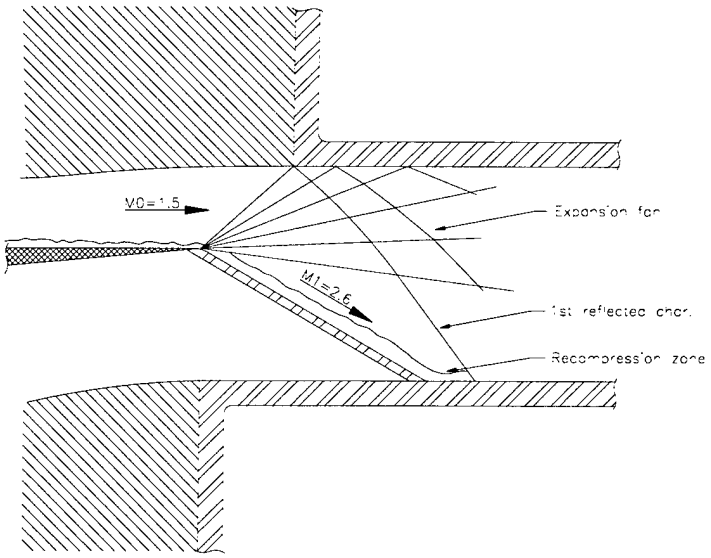

FIG. 15 Schematic of supersonic expansion turn flow, with no mass injection from the porous wall.

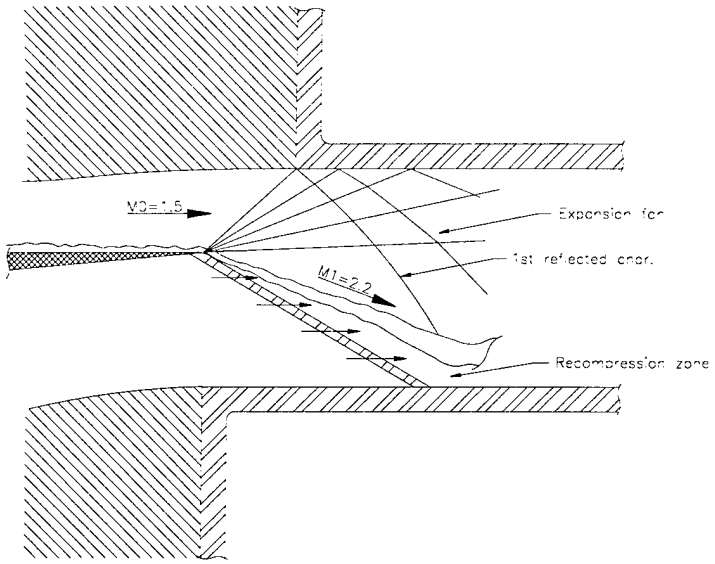

FIG. 16 Schematic of supersonic expansion turn flow, with mass injection from the porous wall. Boundary layer is now lifted from the wall to form a shear layer, entraining the transpiration (lower) injection stream.

As opposed to supersonic flow, where the flow will remain attached over an expansion ramp, in subsonic flow, the flow separates forming a recirculation zone downstream of the ramp. The control of this recirculation zone through mass injection was investigated, taking advantage of variable-geometry effects with no moving parts.

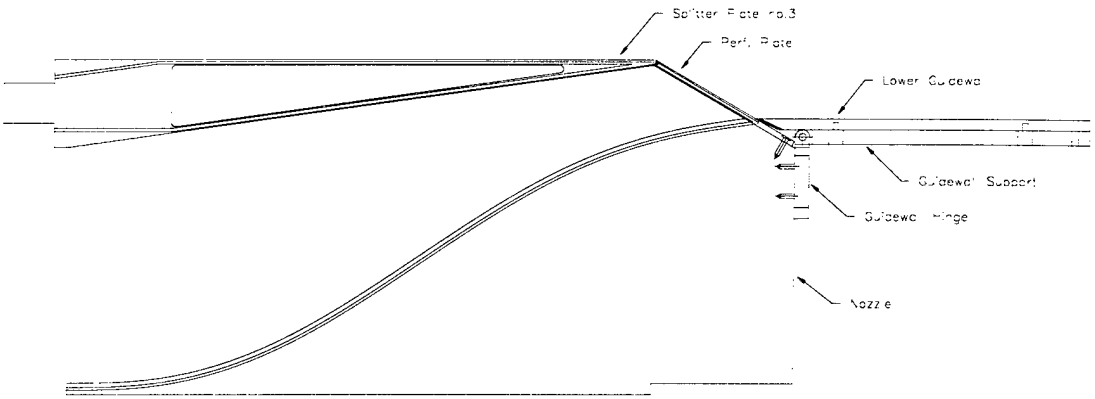

FIG. 17 Supersonic expansion-turn plate assembly.

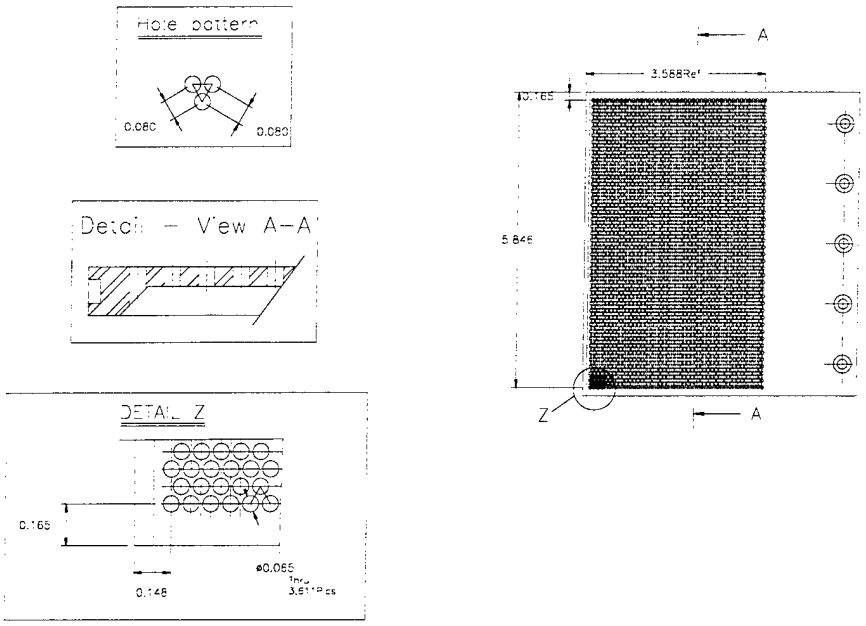

FIG. 18 Supersonic expansion-turn perforated plate (ramp).

A new splitter plate and lower section nozzle block were designed and fabricated as part of this project for use in the GALCIT Supersonic Shear Layer (S^3L) facility. Figure 17 shows the total assembly of the splitter plate, nozzle block, perforated plate, and lower guidewall. A perforated plate was designed for use as the permeable inclined wall in the schematics depicted in Figs. 16 and 17 and is shown in Fig. 18. It has a regular array of 3611 holes of diameter 0.065 in, with an open-area ratio approximately 65%, chosen to avoid the jet-coalescence instability documented by Loehrke & Nagib (1972).

A first set of experiments was conducted with the perforated plate replaced by a solid ramp to determine the reference behavior of the flow with no mass injection. Figure 19 plots normalized streamwise velocity profiles for different maximum freestream velocities. Figure 20 shows a sketch of the variation in the velocity profile as the upstream velocity is increased. Figure 21 plots the normalized velocity, at the fixed measuring station, versus upstream Reynolds number, for the three lowest pitot pressure probes in the test section. This plot suggests that the location of the reattachment point for this flow varies only weakly with Reynolds number. This is not in accord with the conclusion in Song, DeGraaff, & Eaton (2000) who report a reattachment point that is independent of Reynolds number.

A second set of experiments was then performed with injection of a density-matched

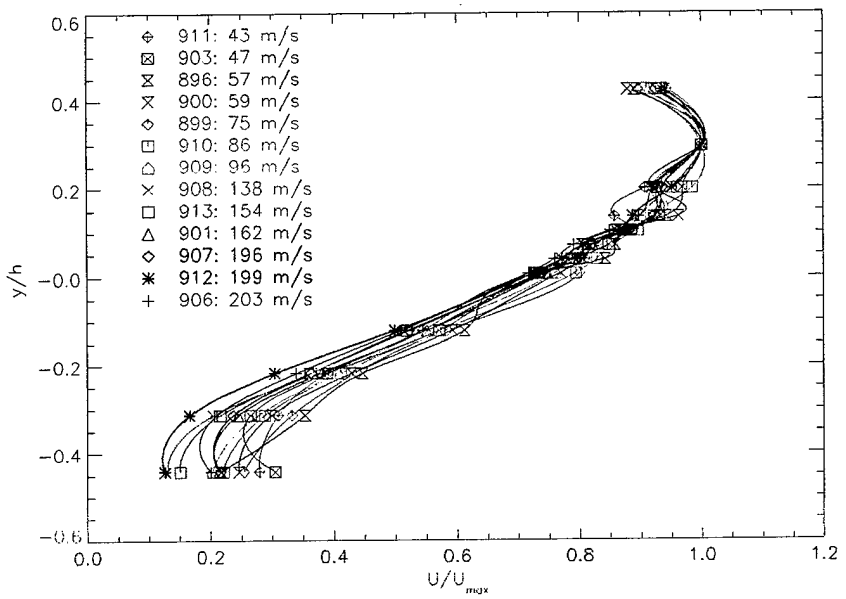

FIG. 19 Normalized streamwise velocity profile for one-stream flow (solid ramp).

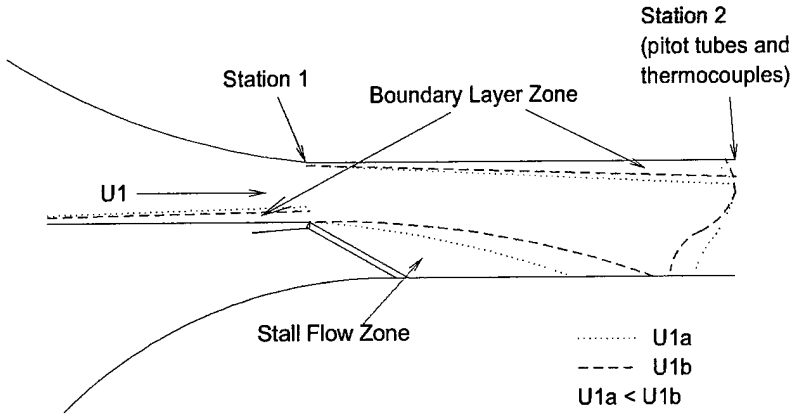

FIG. 20 Schematic of subsonic flow field with no mass injection, showing recirculation zone and downstream measuring station

helium/argon mixture into an upper, high-speed stream of nitrogen. Figure 22 plots the normalized velocity profile for various levels of mass injection of a density-matched He/Ar mixture into the upper, N_2 stream. A run was performed with no mass injection (solid inclined surface), and compared to a run with the same upstream velocity, but with the small mass injection derived from the initial volume of gas in the low-speed plenum (initially at a slightly higher pressure). Subsequent

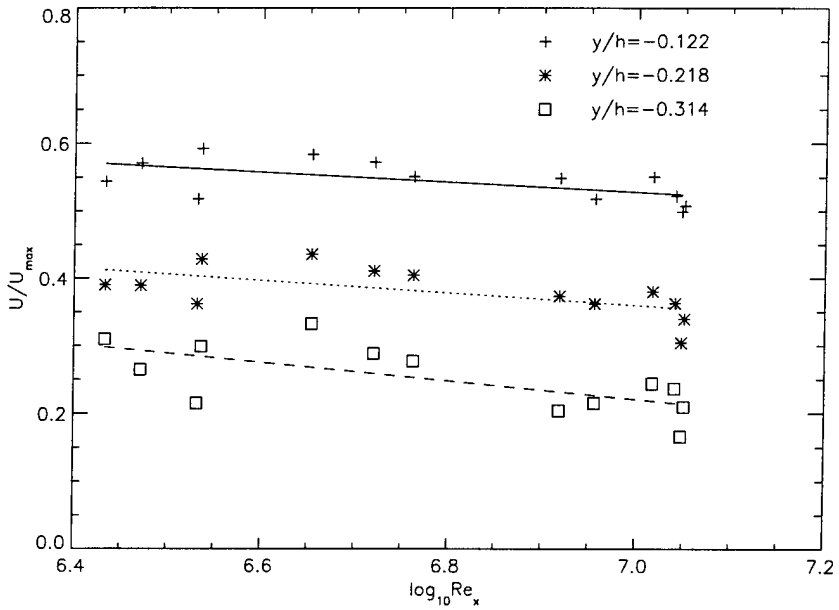

FIG. 21 Normalized velocity on three lowest pitot-pressure measuring probes at the fixed measuring station, *vs. Re*.

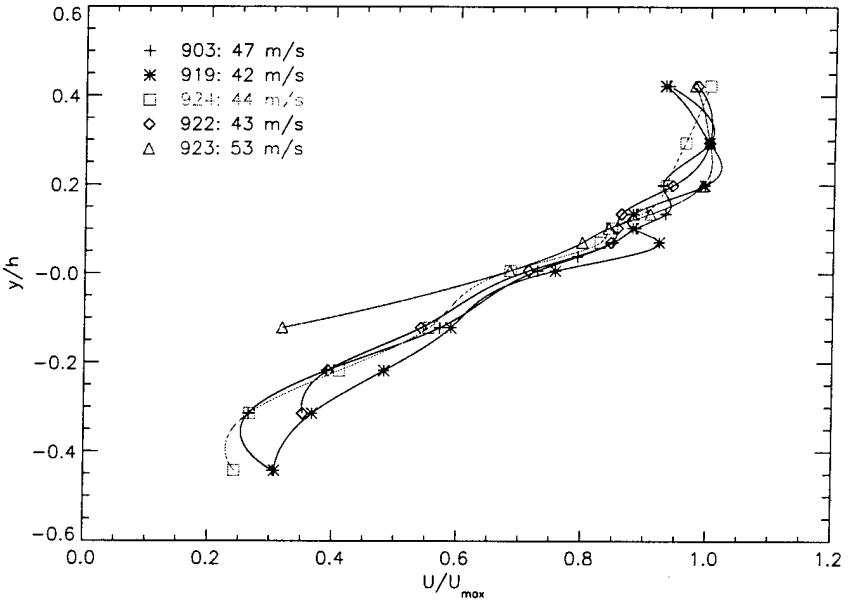

FIG. 22 Normalized streamwise velocity profiles for mass injection of a density-matched He/Ar mixture (see text).

runs were performed with mass injection from the low-speed stream at velocities of 1.8, 6.0, and 18 m/s, respectively. In all cases, the velocity of the upper stream was

FIG. 23 Schlieren visualization of mixing after expansion turn; $U_1 \simeq 55\,\mathrm{m/s}$ [N_2] and $U_2 \simeq 1.8\,\mathrm{m/s}$ [He/Ar].

held constant, the value in the legend representing the maximum velocity achieved at the downstream measuring station. As expected and inferred from these data, the reattachment point moves downstream as the mass injection rate is increased.

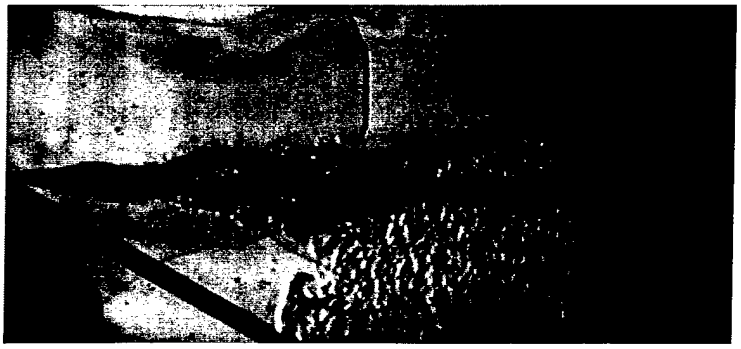

FIG. 24 Schlieren visualization of mixing after expansion turn: $U_1 \simeq 55\,\mathrm{m/s}$ [N_2], $U_2 \simeq 6\,\mathrm{m/s}$ [He/Ar].

Schlieren visualizations were recorded with a 1024^2-pixel, 30 fps CCD camera by Silicon Mountain Design, Model SMD 1M30. Figures 23 and 24 show the upstream flow with $U_1 \simeq 55\,\mathrm{m/s}$, and $U_2 \simeq 1.8\,\mathrm{m/s}$ and $6\,\mathrm{m/s}$, respectively. In these figures, a small region of uniformly mixed fluid is discernible, just downstream of the perforated plate, with a recirculation zone downstream of this region. Figure 25 is a composite of two runs performed with the same inflow, $U_1 \simeq 55\,\mathrm{m/s}$ and $U_2 \simeq 18\,\mathrm{m/s}$, one with the upstream region, the other with the downstream region. In this figure, the transition from a separated region towards a classical shear layer is apparent, with a separated-flow reattachment beyond the measuring station.

FIG. 25 Schlieren visualization of mixing after expansion turn: $U_1 \simeq 55\,\mathrm{m/s}$ [N_2], $U_2 \simeq 18\,\mathrm{m/s}$ [He/Ar].

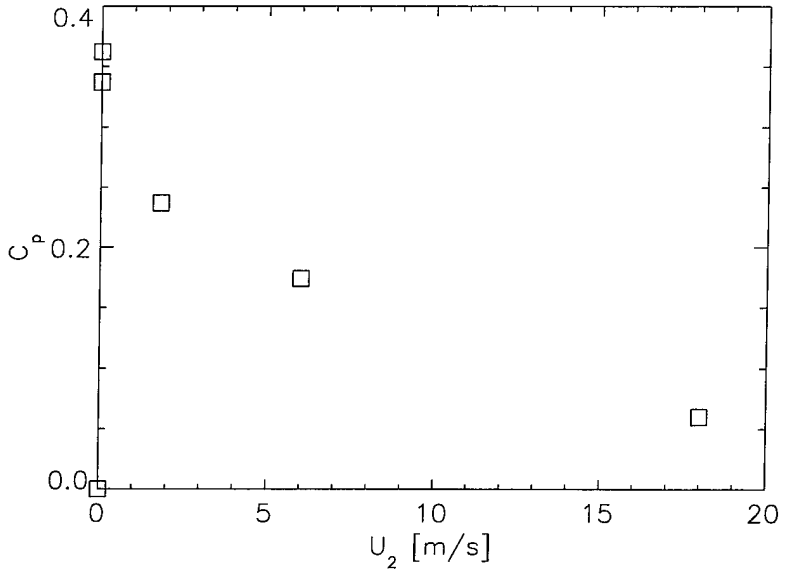

FIG. 26 Internal-flow pressure coefficient (see text) as a function of mass-injection speed.

Many aspects of diffuser operation can be parameterized in terms of a pressure coefficient,

$$C_p = \frac{p_2 - p_1}{\frac{1}{2}\rho U^2} \,. \tag{2}$$

This is plotted in Fig. 26, with Station 1 located on the top guidewall, above the start of the ramp, and Station 2, also on the top guidewall, at the downstream location of the total-pressure-probe array, as indicated in Fig. 20. The two data points at $U_2 = 0$ correspond to flow with no mass injection and small mass injection, from gas already in the lower plenum, whose pressure falls in the course of a run, as

described above. As expected, the pressure coefficient decreases with increasing mass injection, as the reattachment point is pushed further downstream and the flow evolves to form a classical shear layer with a small streamwise pressure gradient (*e.g.*, Dimotakis 1991).

This work is part of the graduate research by Wei-Jen Su and Michael Johnson. It is a precursor to research targeting the performance and control of supersonic internal flows, as would be encountered in hypersonic propulsors. This is presently in progress, as part of work undertaken under AFOSR Grant F49620–01–1–0006.

1.4 Rayleigh-Taylor instability flow

The Rayleigh-Taylor instability (RTI) occurs whenever variable-density flows are subjected to acceleration in a direction opposite that of the density gradient, *e.g.*, as occurs when a heavy fluid finds itself atop a lower-density fluid in a downward gravitational acceleration (*e.g.*, Rayleigh 1883; Taylor 1950; Chandrasekhar 1955, 1961; Duff *et al.* 1962, Sharp 1984). RTI flows arise in a variety of contexts, such as in combustion, rotating-machinery flows, in inertial-confinement fusion, supernovae-explosion flows, geophysical flows, and others. The flow eventually becomes turbulent as secondary (Kelvin-Helmholtz) instabilities develop, increasing, in time, the spectrum of spatial and temporal scales that participate in the dynamics.

Simulation and modeling of RTI flows represents an important test case for hydrodynamic codes, exercising many aspects of turbulence, transport, and diffusion in nonuniform-density flows subject to external body forces. As opposed to homogeneous turbulence in uniform-density flows, RTI flows are driven by a directed internal-force term that is capable of sustaining anisotropy in fully developed flow. Diffusive mixing, which anneals composition (density) differences, plays a dynamic role in this flow and must be captured to represent the dynamics.

RTI models typically assume that the extent, h, of the turbulent mixing zone in the direction of the acceleration, $\mathbf{g}$, following an initial, linear-instability, exponential-growth period, grows quadratically in time (for constant $g = |\mathbf{g}|$), *i.e.*,

$$h(t) \simeq \alpha \mathcal{A} g t^2 \ , \tag{3}$$

where α is accepted as an empirical constant ($0.02 \lesssim \alpha \lesssim 0.08$), and

$$\mathcal{A} \equiv \frac{\rho_2 - \rho_1}{\rho_2 + \rho_1} = \frac{\rho_2/\rho_1 - 1}{\rho_2/\rho_1 + 1} \ , \tag{4}$$

is the Atwood number, with ρ_1 and ρ_2 the densities of the light and heavy fluids across the interface, respectively.

Other parameters for this flow are the Schmidt number (ratio of the kinematic viscosity, ν, to the species diffusivity, $\mathcal{D}$) and the Reynolds number, *i.e.*,

$$Sc \equiv \frac{\nu}{\mathcal{D}} \tag{5}$$

with $\mathcal{D}$ the species diffusivity, and

$$Re \equiv \frac{\rho L U}{\mu} = \frac{L U}{\nu} , \tag{6a}$$

the (outer) Reynolds number, which, for this flow, may be defined as,

$$Re = \frac{h \dot{h}}{\nu} \tag{6b}$$

A host of experimental evidence as well as theoretical arguments indicate that it must be *at least* $1 - 2 \times 10^4$, or so, for the flow to be regarded as *bona fide* turbulent (Dimotakis 1993, 2000).

Direct numerical simulation of RTI flows were performed under the sponsorship of this AFOSR grant, as a collaborative effort with the Caltech ASCI/ASAP program and the Lawrence Livermore National Laboratory (LLNL). A pilot experimental effort was also undertaken, as will be described below.

The numerical simulation effort focused on a study of the incompressible 3-D RTI flow field, computed on the multiprocessor ASCI machines at LLNL by A. Cook (LLNL), followed by quantitative data analysis and 3-D computer visualization by S. Deusch, S. Lombeyda, J. Patton, and P. Dimotakis, at Caltech. Two sets of simulation runs were performed, with the second set attaining a maximum Reynolds number of ≈ 3700, *i.e.*, roughly a third of the mixing-transition value of $Re \approx 10^4$ (Dimotakis 1993, 2000). An illustration of the resulting geometry of the intermediate isosurface from the latter simulations is depicted in Fig. 27.

The boundary conditions for these simulations were space-periodic on the vertical faces of the computational domain, with no-slip on the top/bottom walls. Three cases were run, with different initial-perturbation spectra with peak wavenumbers lower than the most-unstable mode according to the linear-stability analysis of Duff *et al.* (1962), for Case A, comparable, for Case B, and higher for Case C. The initial perturbation spectra were normalized to the same mean-square value for all three runs.

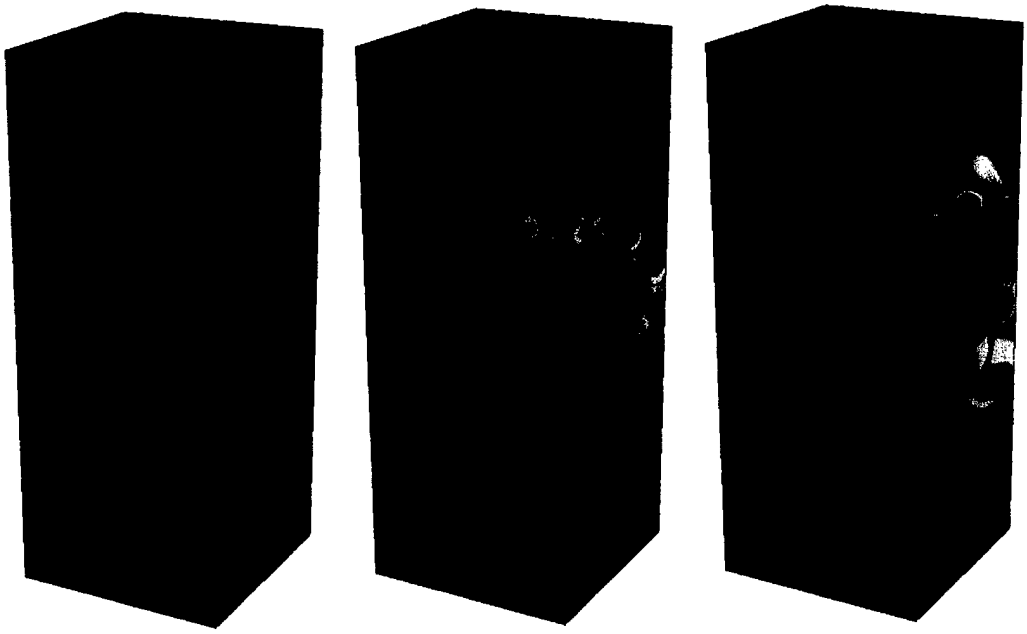

FIG. 27 Time-evolution of intermediate, ($\rho = 2$)-isosurface in Rayleigh-Taylor flow. Pure heavy ($\rho = 3$) fluid is red, pure light ($\rho = 1$) fluid is blue, and the ($\rho = 2$)-isosurface is green. Times for the three images displayed: $t/\tau = 0.0$, 3.44, and 4.63, with $\tau = \sqrt{L/\mathcal{A}g}$ and L the horizontal extent of the flow domain (Cook & Dimotakis 2000a).

Figure 28 depicts the overall extent, $h(t)$, of the RTI mixing zone, along with indicatrices corresponding to $t^{1/2}$ and t^2 growth. Growth during the diffusion-dominated, $h \propto t^{1/2}$, regime is the same for all cases, *i.e.*, independent of the initial perturbations, and in good agreement with analytical predictions for purely diffusive growth. The onset of a second growth stage is conspicuous, with growth that is faster (higher power of t) than diffusive. This occurs at a different time for each of the three cases, reflecting differences in the initial modal seeding in each case. Available linear-stability analysis (Duff *et al.* 1962) does not account for the order in which the growth breaks out of the diffusive regime. Also, as can be seen, only Case C, which was seeded with the highest wavenumber initial disturbances, appears to grow approximately quadratically. Cases A and B do not support the conventional modeling of this phenomenon.

Analysis of the results yielded statistics for Taylor microscales, indicating that the

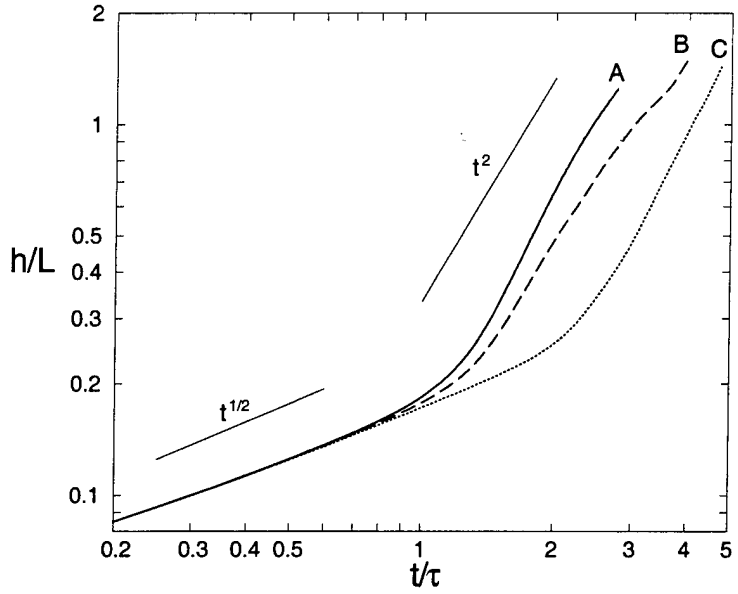

FIG. 28 Mixing-zone extent, h/L, *vs.* t/τ, for the three cases (Cook & Dimotakis 2000a).

directed buoyancy force that drives this flow sustains an anisotropic field, precluding the use of standard turbulence theory. Values were found to be similar in scaling and magnitude to ones measured in high Reynolds number turbulent jets.

A summary presentation of results from this work was made at the ICTAM 2000 meeting (Cook & Dimotakis 2000b). A first documentation of this work was issued as an LLNL report and, revised, subsequently submitted for publication to the *J. Fluid Mechanics* (Cook & Dimotakis 2000a).

A preliminary experimental investigation of the Rayleigh-Taylor instability was also undertaken as part of this work. The investigation spans the experimental process from conceptual and experimental design to the execution of a set of experiments tailored to capture a flow that is very difficult to probe.

The design and fabrication of a new pilot facility was completed. This design adapted and improved upon an established method for keeping two fluids in an unstable configuration prior to flow initiation (Dalziel *et al.* 1999). Two experiments were successful, at an Atwood number, $\mathcal{A} \simeq 1.26 \times 10^{-4}$ (Eq. 4), with results in reasonable accord with previous experiments.

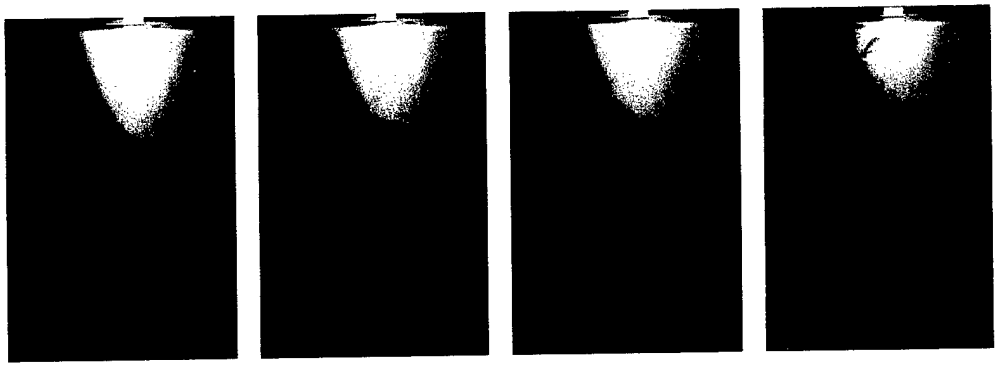

FIG. 29 Laser-induced fluorescence images of Rayleigh-Taylor instability ($\mathcal{A} = 1.26 \times 10^{-4}$). Experiment A.

Flow visualization was performed using laser-induced fluorescence with sodium fluorescein, at a dye concentration of 4.18×10^{-4} g/L (molar concentration of 1.11×10^{-6} M), in the top chamber, and an argon-ion laser as the excitation source. Images were acquired using the Caltech-developed Cassini digital-imaging system (see Sec. 1.6).

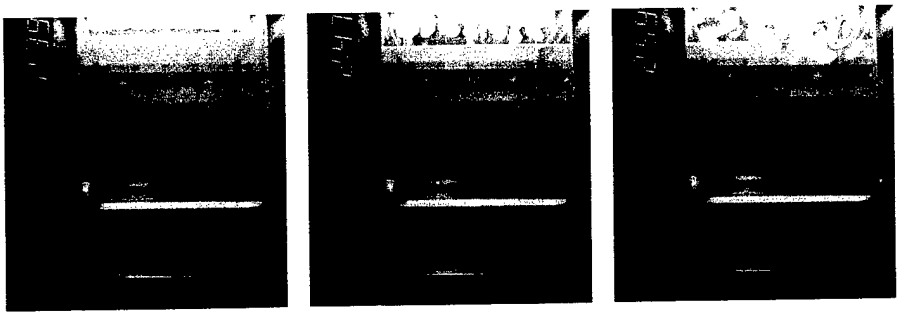

FIG. 30 Laser-induced fluorescence images of Rayleigh-Taylor instability ($\mathcal{A} = 1.26 \times 10^{-4}$). Experiment B (see text).

Figure 29 shows the evolution of a well-developed Rayleigh-Taylor mixing zone. This was recorded approximately 18 s after the retraction of the partition. As can be seen, the instability thickness above and below the interface is approximately the same, with the four, or five structures arranged in an alternating pattern. Similar inferences can also be drawn from Fig. 30.‡ Following Sharp (1984), the flow can

‡ The images in Fig. 30 were extracted from a sequence recorded with the optical axis below the original interface level, to avoid obtrusion by the groves that guide the separation-plate assembly (*cf.* Fig. 29), while maintaining an optical axis perpendicular to the test-section vertical wall, to avoid perspective distortions. As a consequence, the developing Rayleigh-Taylor layer is seen near the top of the field of view.

be characterized as having evolved well into Stage 2 (penetration) of the instability. Also apparent in most of the structures are roll-ups, or "mushroom caps", with enhanced mixing at the roll-up interfaces. Time-histories of mixing-zone height, top-/bottom-layer penetration, and mean thickness of the developing flow are shown in Fig. 31. In 12.7 s from the instant the separator trailing edge passed the laser sheet, the interface height dropped 10 mm. The growth of the RTI mixing zones was found to exhibit an approximately quadratic dependence on time, in reasonable accord with Eq. 3.

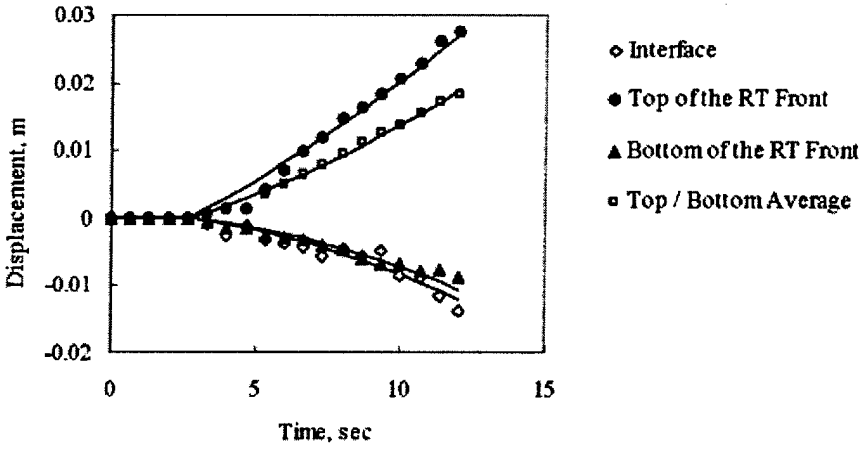

FIG. 31 Displacement time-histories for the interface, both sides of the RTI front, and their average ($\mathcal{A} = 1.26 \times 10^{-4}$).

Using the model in Eq. 3, curve fits with an adjustable origin in time, as required by the data, are shown in Fig. 31. The data are consistent with an approximate value of the model constant of $\alpha \simeq 0.6$, with varying values for the time origin, t_0. This value of α is in reasonable accord with previously published values.

The maximum Reynolds number attained in these experiments (Eq. 6b) was modest, in particular, considerably smaller than values required to place the flow in the fully developed turbulence regime (Dimotakis 2000). Higher values would have to be attained if the influence of turbulent mixing on this density-difference-driven flow are to be documented.

This part of the work was performed by Jimmy Fung and Wei-Jen Su and was partly supported by the Caltech ASCI/ASAP program (DOE Grant W–7405–ENG–48).

1.5 Advances in Image Correlation Velocimetry

The work also advanced Image Correlation Velocimetry (ICV: Tokumaru & Dimotakis 1995, Gornowicz 1997), which extracts velocity-field information from successive images of any Lagrangian markers (particles, dye, *etc.*). In a collaborative effort with R. Pitz (Vanderbilt), it was applied to Lagrangian flow-tagging techniques (Ozone-tagging Velocimetry (OTV), or hydroxyl-tagging velocimetry (HTV)) for low- and high-temperature gas-phase flows (Pitz *et al.* 1998, Wehrmeyer *et al.* 1999).

In these techniques, a laser-beam grid is applied using a 193 nm ArF excimer laser to produce lines of ozone in an air stream (OTV), or hydroxyl radicals in a burning hydrocarbon flame (HTV). These species fluoresce and can be used to mark advection of the grid by laser induced fluorescence (LIF), using a 248 nm KrF laser. ICV is then used to infer the velocity field from two realizations of the advected LIF grid (Fig. 32).

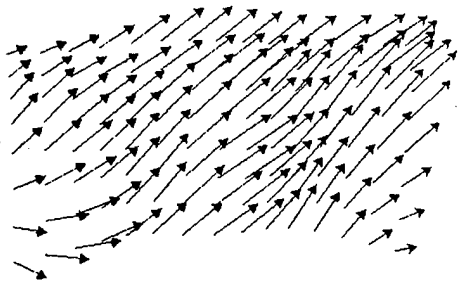

FIG. 32 Image Correlation Velocimetry application to O_3-tagged grid. Arrows denote in-plane velocity field vectors of gas-phase flow, $u \simeq 5-7\,\mathrm{m/s}$. Underlying grey-scale image depicts the superposition of the initial and advected grid of the fluorescing O_3 streaks.

In other related work in ICV, a collaboration with Ö. Savas (Berkeley) was undertaken to provide a quantitative assessment of ICV, Lagrangian Particle Tracking (LPT; Sholl & Savas 1997), and other PIV methods. A paper documenting this study was recently submitted for publication (Deusch *et al.* 2000). The work on ICV is part of the research effort by S. B. Deusch, in collaboration with P. Dimotakis.

1.6 Advances in digital-imaging and high-speed data acquisition

Phase 1 of a multi-year project on high-performance digital-imaging development was completed. The new system has been dubbed the KFS system, after its kilo-frame-per-second framing-rate specification, and represents a substantial enhancement of our previous-generation Cassini system.

The Cassini system relies on CCD's developed for the NASA Cassini mission, developed by J. Janesick,[♯] M. Wadsworth, S. A. Collins, S. T. Elliott, and others, of the JPL Space Instrumentation Implementation Section. The Cassini system camera head and data acquisition electronics were designed and integrated by Dan Lang, in collaboration with Pavel Svitek and Paul Dimotakis at Caltech. The Cassini system is capable of 10 fps (frames per second), at up to 12 bits/pixel at 1024^2-pixel frame resolution, or 20 fps at 512^2-pixel frames, which even though completed several years ago, remains ahead of commercially available systems, in terms of its combination of spatial resolution, dynamic range (SNR), and framing rate. It was used in the transverse-jet mixing studies (Sec. 1.2) and is presently in use in the hydrocarbon-flame studies (Sec. 1.1.2), under sponsorship of the current AFOSR F49620–01–1–0006 grant.

Initially under AFOSR/DURIP Grant F49620–95–1–0199, Phase 1 of the KFS system was completed as part of this program, with some additional support from the AFOSR Grant F49620–00–1–0036 on Aerooptics studies, with which the development and use of this equipment is shared. It should be noted that digital imaging has been part of all the experimental efforts under this grant. Those continuing under current AFOSR sponsorship (Sec. 1.2) await the next developments for their completion.

The KFS system is designed to record 1024^2-pixel frames, at 12-bits/pixel, at rates as high as 10^3 fps (frames/sec), for an aggregate data rate as high as 10^9 measurements/s. Its signal-to-noise ratio exceeds anything available commercially or otherwise at comparable resolution and framing rates.* The KFS CCD was designed in collaboration with JPL (M. Wadsworth, S. A. Collins, and S. T. Elliott) and fabricated by Lockheed Martin (Milpitas, Palo Alto). The camera head, electronics, data-acquisition system, and computer interface hardware, firmware, and software

---

♯ Now with PixelVision, Inc.

* The conversion dynamic range is programmable, with 13, 14, 15, or 16 bits/pixel at lower framing rates.

were designed and fabricated at Caltech by Dan Lang. Other KFS system design and components were developed in collaboration with Pavel Svitek (Aeronautics), Steve Kaye (Physics), Brian Kern (Astronomy), and Paul Dimotakis.

In its present implementation (Phase 1), the system is capable of 160 fps, corresponding to 1.6×10^8, 12-bit measurements/s. At this rate, it can record 4000 to 12,000 frames, depending on data signal-to-noise ratio by utilizing a front-end, lossless data compression, before offloading to hard-disk storage. At $25 - 50$ fps, it can record for minutes. Upgrades in progress will increase the rate to its 1000 fps (Phase 2) and, subsequently, its recording capacity at the highest rate to millions of frames (Phase 3).

It was preliminarily used (prior to Phase 1 completion) on the 200″ Palomar telescope (May 2000) for atmospheric-turbulence/aerooptics measurements using a bright star as a reference (with Prof. Chris Martin and Brian Kern; Caltech Astronomy/Physics). At present, further increases in high-framing rate LIF applications would be limited by available high-energy, high-quality-beam, pulsed lasers. Long-term experimental goals include 3-D unsteady measurements in turbulence and mixing, combustion, aerooptics, and many other areas. This is a vital technology development, broadly useful to many other areas, both within and outside AFOSR and DoD interests.

1.7 Conclusions

The research in this program is comprised of several inter-related parts.

The numerical-simulation (Sec. 1.1.1) and experimental studies (Sec. 1.1.2) of hydrocarbon flames are motivated by the need to characterize hydrocarbon flames under variable strain-rate conditions. Such conditions are encountered in anticipated SCRAMJET-propulsor configurations and complex-geometry internal flows, which are the object of the studies outlined in Sec. 1.3. In SCRAMJETs, in turn, many fuel-injection scenaria anticipate transverse-jet configurations, which were studied as outlined in Sec. 1.2. Injected fuel can be in the form of droplets; sphere/droplet wakes in the relevant Reynolds-number range, the first part of a study of which is in ??, which continues under our current AFOSR grant F49620–01–1–0006. Flow with density inhomogeneities that is subject to acceleration forces in the direction of density gradients — virtually assured in inhomogeneous turbulent flow in both internal and rotating-machinery flows — is subject to the Rayleigh-Taylor instability.

This has been the subject of investigations in other communities, but not by much of the fluid-dynamics community. It is the subject of direct-numerical simulation and a preliminary experimental effort, as outlined in Sec. 1.4.

Our modeling of hydrocarbon flames and combustion led to the computational and experimental work on low-C hydrocarbon flames (Sec. 1.1) and highlighted significant deficiencies in the ability to simulate such phenomena. Low-C hydrocarbons are the product of thermal cracking, either in flames or as anticipated in the endothermic use of the fuel in hypersonic vehicles. Their relation to ignition, flame stability, and extinction are important to air-breathing propulsion, in particular, and the AFOSR mission, in general. Under continuing AFOSR support, we are presently engaged in a program to address these deficiencies as well as provide a substantial increase in the available experimental database to assist in the improvement and validation of chemical-kinetics models. A first presentation (Vagelopoulos & Dimotakis 2001) of our results will take place at the up-coming 2nd U.S. Joint Meeting (25–28 March 2001, Oakland, CA).

At this time, much, if not most, of turbulence theory relies on assumptions of (at least, local) isotropy and homogeneity to reduce the number of variables that must be modeled. Our work on transverse jets (Sec. 1.2), an important flow in its own right and in many high-speed air-breathing propulsion and turbulent-mixing contexts, as noted above, highlighted the need for descriptions of turbulence that do not rely on these assumptions.

The same conclusion was arrived at on the basis of studies of Rayleigh-Taylor-instability flow (Sec. 1.4), as well as a host of others on mixing. The latter illustrated significant similarities with mixing in high-Re shear layers as well as with turbulent microscale behavior of turbulent jets. One of the largest direct-numerical simulations of this phenomenon was conducted as part of this study, relying on the full Navier-Stokes equations, including molecular diffusion between the two participating fluids. It was undertaken in collaboration with the Lawrence Livermore National Laboratory and performed on DOE's ASCI computers.

Advances were also realized in flow-field velocimetry (Sec. 1.5), based on previous work on Image Correlation Velocimetry, as well as on high-performance digital-imaging technology (Sec. 1.6). These developments are crucial to the success of several AFOSR-supported research projects at this time, under AFOSR grants F49620–00–1–0036 and F49620–01–1–0006.

The research program undertaken as part of this grant was very productive. A large number of publications, reports, presentations, interactions and collaborations stemmed from it, as outlined in Secs. 4 and 5.

2. References

ANTONIA, R.A., BROWNE, L.W.B., BRITZ, D. & CHAMBERS, A.J. 1984 A comparison of properties of temporal and spatial temperature increments in a turbulent plane jet. *Phys. Fluids* **27**(1), 87–93.

AXELROD, D., KOPPEL, D.E., SCHLESSINGER, J., ELSON, E. & WEBB, W.W. 1976 Mobility measurement by analysis of fluorescence photobleaching recovery kinetics. *Appl. Phys. Lett* **16**, 1055–1069.

BOWMAN, C. T., FRENKLACH, M., GARDINER, W. R. & SMITH, G. 1999 The 'GRI 3.0' Chemical Kinetic Mechanism. `http://www.me.berkeley.edu/gri_mech/`.

CATRAKIS, H. J. & DIMOTAKIS, P. E. 1996 Mixing in turbulent jets: scalar measures and isosurface geometry. *J. Fluid Mech.* **317**, 369–406.

CHANDRASEKHAR, S. 1955 The character of the equilibrium of an incompressible heavy viscous fluid of variable density. *Proc. Cambridge Phil. Soc.* **51**, 162–178.

CHANDRASEKHAR, S. 1961 *Hydrodynamic and Hydromagnetic Stability.* Oxford University Press. Republished by Dover Publications, New York, 1981.

CHING, E.S.C. 1991 Probabilities for temperature differences in Rayleigh-Benard convection. *Phys. Rev.* A **44**, 3622–3629.

CLIFT, R., GRACE, J. R. & WEBER, M. E. 1978 *Bubbles, Drops, and Particles.* Academic Press, New York.

COOK, A. W. & DIMOTAKIS, P. E. 2000a Transition stages of Rayleigh-Taylor instability between miscible fluids. LLNL Report No. UCRL–JC–139044. *J. Fluid Mech.* (submitted).

COOK, A. W. & DIMOTAKIS, P. E. 2000b Investigation of mixing effects in incompressible Rayleigh-Taylor instability. 20^{th} *IUTAM Congress*, Paper GK06.

DALZIEL, S. B., LINDEN, P. F. & YOUNGS, D. L. 1999 Self-similarity and internal structure of turbulence induced by Rayleigh-Taylor instability. *J. Fluid Mech.* **399**, 1–48.

DANDY, D. S. & LEAL, G. L. 1989 Buoyancy-driven motion of a deformable drop through a quiescent liquid at intermediate Reynolds numbers. *J. Fluid Mech.* **208**, 161–192.

DEUSCH, S. B., GORNOWICZ, G. G., DIMOTAKIS, P. E. & SAVAS, O. 2000 Continuous Image Correlation Velocimetry optimization based on B-Splines. *Exps. in Fluids* (submitted).

DIMOTAKIS, P. E. 2000 The mixing transition in turbulence. *J. Fluid Mech.* **409**, 69–98.

DIMOTAKIS, P. E. 1991 Turbulent Free Shear Layer Mixing and Combustion. *High Speed Flight Propulsion Systems*, in *Progress in Astronautics and Aeronautics* **137**, Ch. 5, 265–340.

DIMOTAKIS, P. E. 1993 Some issues on turbulent mixing and turbulence. GALCIT Report FM93–1a.

DIMOTAKIS, P. E., DEBUSSY, F. D. & KOOCHESFAHANI, M. M. 1981 Particle streak velocity field measurements in a two-dimensional mixing layer. *Phys. Fluids* **24**(6), 995–999.

DUFF, R. E., HARLOW, F. H. & HIRT, C. W. 1962 Effects of Diffusion on Interface Instability Between Gases. *Phys. Fluids* **5**, 417–425.

EDWARDS, T. 1996 Fuels and Fuel System Area: Air Force Perspective. AFOSR/-NASA Workshop on Supersonic Scramjet Combustion (13–16 May 1996, Newport News, VA).

EGOLFOPOULOS, F. N. & CAMPBELL, C. S. 1996 Unsteady, counterflowing, strained diffusion flames: frequency response and scaling. *J. Fluid Mech.* **318**, 1–29.

EGOLFOPOULOS, F. N. & DIMOTAKIS, P. E. 2000a Effects of additives on the non-premixed ignition of ethylene in air. *Combust. Sci. and Technol.* **156**, 173–199.

EGOLFOPOULOS, F. N. & DIMOTAKIS, P. E. 2000b A comparative study of ethylene kinetics in premixed and non-premixed flames. *Combust. Sci. and Technol.* (in press).

EGOLFOPOULOS, F. N. & DIMOTAKIS, P. E. 1998 Non-premixed hydrocarbon ignition at high strain rates. *Proc. Combustion Inst.* **27**, 641–648.

EGOLFOPOULOS, F. N., DIMOTAKIS, P. E. & BOND, C. L. 1996 On Strained Flames with Hypergolic Reactants: The $H_2/NO/F_2$ System in High-Speed, Supersonic and Subsonic Mixing-Layer Combustion. *Twenty-Sixth Symposium (International) on Combustion.* The Combustion Institute, Pittsburgh, 2885–2893.

FAETH, G. M. 1983 Evaporation and Combustion of Sprays. *Prog. Energy Combust. Sci.* **9**, 1–76.

FRENKLACH, M., WANG, H., GOLDENBERG, M., SMITH, G. P., GOLDEN, D. M., BOWMAN, C. T., HANSON, R. K., GARDINER, W. C. & LISSIANSKI, V. 1995 The GRI 2.1 Chemical Kinetic Mechanism. `http://www.me.berkeley.edu/gri_mech/`.

GILBRECH, R. J. 1991 *An Experimental Investigation of Chemically-Reacting, Gas-Phase Turbulent Jets.* Ph.D. thesis, California Institute of Technology.

GILBRECH, R. J. & DIMOTAKIS, P. E. 1992 Product Formation in Chemically Reacting Turbulent Jets. *AIAA* 30^{th} *Aerospace Sciences Meeting*, Paper 92–0581.

GOLDIN, G.M. & MENON, S. 1997 A scalar PDF construction model for turbulent non-premixed combustion. *Combust. Sci. and Technol.* **125**, 47–72.

GORNOWICZ, G. G. 1997 *Continuous-field Image-Correlation Velocimetry and its Application to Unsteady Flow Over an Airfoil.* California Institute of Technology, AeE thesis.

KEE, R. J., GRCAR, J. F., SMOOKE, M. D. & MILLER, J. A. 1985 A Fortran program for modeling steady laminar one-dimensional premixed flames. SAND85-8240 DoE report.

KEE, R. J., RUPLEY, F. M. & MILLER J. A. 1989 Chemkin-II: A Fortran Chemical Kinetics Package for the Analysis of Gas-Phase Chemical Kinetics. Sandia Report SAND89–8009.

KEE, R. J., WARNATZ, J. & MILLER, J. A. 1983 A FORTRAN Computer Code Package for the Evaluation of Gas-Phase Viscosities, Conductivities and Diffusion Coefficients. Sandia Report SAND83–8209.

LAW, C. K. 1982 Recent Advances in Droplet Vaporization and Combustion. *Prog. Energy Combust. Sci.* **8** 171–201.

LOEHRKE, R. I. & NAGIB, H. M. 1972 Experiments on Management of Free-Stream Turbulence. AGARD–R–598.

MARINOV, N. 1999 A Detailed Kinetic Model for High Temperature Ethanol Oxidation. *Int. J. Chem. Kinet.* **31**(3), 183–220.

MARINOV, N., PITZ, W., WESTBROOK, C., HORI, M. & MATSUNAGA, N. 1998 An Experimental and Kinetic Calculation of the Promotion Effect of Hydrocarbons on the NO-NO_2 Conversion in a Flow Reactor. *Twenty-Seventh Symposium (International) on Combustion.* The Combustion Institute, Pittsburgh, 389–396.

MATHUR, T., BILLIG, F., STREBY, G., GRUBER, M., JACKSON, K., DONBAR, J., DONALDSON, W., JACKSON, T. & SMITH, C. 1999 Supersonic combustion experiments with a cavity-based fuel injector. 35^{th} *AIAA/ASME/SAE/ASEE Joint Propulsion Conference and Exhibit* (20–24 June 1999, Los Angeles, California).

MYDLARSKI, L. & WARHAFT, Z. 1998 Three-point statistics and the anisotropy of a turbulent passive scalar. *Phys. Fluids* **10**(11), 2885–2894.

PITZ, R. W., RIBAROV, L. A., WEHRMEYER, J. A. & BATLIWALA, F. 1998 Ozone Tagging Velocimetry for Unseeded Velocity Measurements in Air Flows. *AIAA* 20^{th} *Advanced Measurement and Ground Testing Technology Conference*, Paper 98–2610.

POPE, S. B. 1985 PDF Methods for Turbulent Reactive Flows. *Prog. Energy Comb. Sc.* **11**, 119–192.

RAYLEIGH, LORD 1883 Investigation of the character of the equilibrium of an incompressible heavy fluid of variable density. *Proc. London Math. Soc.* **14**, 170–177.

SHAN, J. W. 2001 *Mixing and Isosurface Geometry in Turbulent Tranverse Jets.* California Institute of Technology, Ph.D. thesis.

SHAN, J. W. & DIMOTAKIS, P. E. 2000 Turbulent scalar mixing in transverse jets. *Am. Phys. Soc.*, 53^{nd} *Annual Meeting, Division of Fluid Dynamics*, (19–21 November 2000, Washington, DC), Abstract BB.007.

SHAN, J. W. & DIMOTAKIS, P. E. 2001 Turbulent mixing in liquid-phase transverse jets. (in preparation).

SHARP, D. H. 1984 An overview of Rayleigh-Taylor instability. *Physica* D **12**, 3–18.

SHOLL, M. & SAVAS, Ö. 1997 A Fast Lagrangian PIV Method for Study of General High-Gradient Flows. *AIAA* 35^{th} *Aerospace Sciences Meeting*, Paper 97–0493.

SIRIGNANO, W. A. 1983 Fuel Droplet Vaporization and Spray Combustion Theory. *Prog. Energy Combust. Sci.* **9**, 291–322.

SIRIGNANO, W. A. 1993 Fluid Dynamics of Sprays – 1992 Freeman Scholar Lecture. *J. Fluids Eng.* **115**, 345–377.

SONG, S., DEGRAAFF. D. B. & EATON, J. K. 2000 Experimental study of a separating, reattaching, and redeveloping flow over a smoothly contoured ramp. *Int. J. Heat and Fluid Flow* **21**(5), 512–519.

TAN, Y., DAGAUT, P., CATHONNET, M., BOETTNER, J. C., BACHMAN, J. S. & CARLIER, P. 1994 Natural Gas and Blends Oxidation and Ignition: Experiments and Modeling. *Proc. Combustion Inst.* **25**, 1563–1569.

TAYLOR, G. I. 1950 The instability of liquid surfaces when accelerated in a direction perpendicular to their planes. *Proc. Roy. Soc. London* A **201**, 192–196.

TOKUMARU, P. T. & DIMOTAKIS, P. E. 1995 Image Correlation Velocimetry. *Exps. in Fluids* **19**(1), 1–15.

VAGELOPOULOS, C. M. 1999 *An experimental and numerical study on the propagation and stability of laminar premixed flames.* Ph.D. thesis, U. So. California.

VAGELOPOULOS, C. M. & DIMOTAKIS, P. E. 2001 Rapid recording of flame propagation and extinction behavior in methane-air mixtures. 2nd U.S. Joint Meeting (Combustion Institute), 25–28 March 2001 (Oakland, CA), Paper 136..

WALKER, D.A. 1987 A fluorescence technique for measurement of concentration in mixing liquids. *J. Phys. E.: Sci. Instrum.* **20**, 217–224.

WANG, H. & FRENKLACH, M. 1997 A Detailed Kinetic Modeling Study of Aromatics Formation in Laminar Premixed Acetylene and Ethylene Flames. *Comb. and Flame* **110**, 173–221.

WANG, H., LASKIN, A., DJURISIC, Z. M., LAW, C. K., DAVIS, S. G. & ZHU, D. L. 1999 A Comprehensive Mechanism of C2Hx and C3Hx Fuel Combustion. *Chemical and Physical Processes of Combustion* (Fall Technical Meeting of the Eastern States Section of the Combustion Institute, Raleigh, NC), 129–132.

WEHRMEYER, J. A., RIBAROV, L. A., OGUSS, D. A. & PITZ, R. W. 1999 Flame flow tagging velocimetry with 193-nm H_2O photodissociation. *Appl. Optics* **38**, 6912–6917.

3. Personnel

3.1 Research personnel supported under this grant

- Bergthorson, J. M., Graduate Research Assistant, Aeronautics (starting June 2000).
- Bond, C. L., Graduate Research Assistant, Aeronautics (through June 1999).
- Dahl, E. E., Member of the Technical Staff, Aeronautics.
- Deusch, S. B., Post-Doctoral Scholar, Aeronautics (through 30 April 2000).
- Dimotakis, P. E., John K. Northrop Professor of Aeronautics & Professor of Applied Physics (PI).
- Egolfopoulos, F. N., Associate Professor, Mech. Eng., U. Southern California. Also, Visiting Research Associate, Aeronautics, Caltech.
- Fung, J., Graduate Research Assistant, Aeronautics.
- Gargas, D., Summer Undergraduate Research Fellow, Aeronautics (summer 2000).
- Hwang, A., Summer (High-School) Research Intern (Summer 2000).
- Johnson, M. B., Graduate Research Assistant, Aeronautics (starting June 2000).
- Lang, D. B., Research Engineer, Aeronautics.
- Leonard, A., Theodore von Karman Professor of Aeronautics (Co-PI).
- Malhotra, S., Graduate Research Assistant, Aeronautics.
- Metcalf, R., Undergraduate Research Assistant, Mechanical Engineering (summer 2000).
- Papalexandris, M. V., originally as Graduate Research Assistant, Aeronautics. Presently with the Jet Propulsion Laboratory (since March 1998). Continued on authoring work previously supported under this grant.
- Shan, J. W., Graduate Research Assistant, Aeronautics.
- Slessor, M. D., Graduate Research Assistant, Aeronautics (through June 1998).
- Su, W.-J., Graduate Research Assistant, Aeronautics.

- Svitek, P., Staff Engineer. Aeronautics. (through 31 March 2000).
- Vagelopoulos, C. M., Post-Doctoral Scholar, Aeronautics.
- Wang, C.-F., Graduate Research Assistant, Aeronautics (June 2000 through December 2000).

3.2 Other collaborators

- Cook, A. W., Lawrence Livermore National Laboratory. Collaborator on direct numerical simulations of three-dimensional, variable-density flows.
- Cook, G., Lawrence Livermore National Laboratory. Collaborator on direct numerical simulations of variable-density flows and flows with strong fronts.
- Collins, S. A., JPL (digital imaging; KFS development).
- Elliott, S. T., JPL (digital imaging; KFS development).
- Gornowicz, G. G., DreamWorks SKG (Glendale, CA), continuing informal collaborator in our ICV effort.
- Kern, Brian, Graduate Research Assistant, Astronomy, Caltech. Collaborator in the high framing-rate imaging (KFS) development.
- Lombeyda, S., Member of the Technical Staff, Center for Advanced Computing Research, Caltech. Collaborator on 3-D computer visualization.
- Martin, C., Prof. Physics, Caltech. Collaborator in the high framing-rate imaging (KFS) development.
- Meiron, D. I., Prof. Applied Mathematics, Caltech. Collaborator, on direct-numerical simulations of 3-D, variable-density flows.
- Miller, P. L., Lawrence Livermore National Laboratory. Collaborator on turbulent mixing in a variety of compressible- and incompressible-turbulence contexts.
- Patton, J. M., Member of the Technical Staff, Center for Advanced Computing Research (CACR), Caltech. Collaborator on high-capacity data storage and 3-D computer visualization.
- Peyser, T., Lawrence Livermore National Laboratory. Collaborator on turbulent mixing in a variety of compressible- and incompressible-turbulence contexts.

- Pitz, R. W., Mechanical Engineering, Vanderbilt University. Collaborator on Image Correlation Velocimetry (ICV) applications using excited ozone and hydroxyl Lagrangian markers in gas-phase flows.
- Savas, O., Mechanical Engineering, U. C. Berkeley. Collaboration on ICV technology and characterization.
- Wadsworth, M., JPL (digital imaging). Principal designer of kilo-frame/sec (KFS) CCD focal-plane array.

4. Publications and reports of work supported under this Grant

Publications, submissions and acceptances for publication, presentations, or reports of work performed under sponsorship of this grant.

BOND, C. L. 1999 *Reynolds Number Effects on Mixing in the Turbulent Shear Layer*. Ph.D. thesis, California Institute of Technology.

CATRAKIS, H. J. & DIMOTAKIS, P. E. 1998 Shape Complexity in Turbulence. *Phys. Rev. Lett.* **80**(5), 968–971.

COOK, A. W. & DIMOTAKIS, P. E. 1999 Direct Numerical Simulation of Rayleigh-Taylor Instability. *Am. Phys. Soc.*, 52$^{\text{nd}}$ *Annual Meeting, Division of Fluid Dynamics*, (21–23 November 1999, New Orleans, LA), DN.03.

COOK, A. W. & DIMOTAKIS, P. E. 2000 Transition stages of Rayleigh-Taylor instability between miscible fluids. LLNL Report No. UCRL–JC–139044. *J. Fluid Mech.* (submitted).

COOK, A. W. & DIMOTAKIS, P. E. 2000 Investigation of mixing effects in incompressible Rayleigh-Taylor instability. 20$^{\text{th}}$ *IUTAM Congress*, 22 August – 2 September 2000 (Chicago, IL), Paper GK06.

DEUSCH, S. B., GORNOWICZ, G. G., DIMOTAKIS, P. E. & SAVAS, O. 2000 Continuous Image Correlation Velocimetry optimization based on B-Splines. *Exps. in Fluids* (submitted).

DIMOTAKIS, P. E. 2000 The mixing transition in turbulence. *J. Fluid Mech.* **409**, 69–98.

DIMOTAKIS, P. E. 2000 Recent Advances in Turbulent Mixing. 20th *IUTAM Congress*, 22 August – 2 September 2000 (Chicago, IL), Invited sectional lecture, Paper EW1. Available as CIT–ASCI–TR065.

DIMOTAKIS, P. E., CATRAKIS, H. J., COOK, A. W. & PATTON, J. M. 1998 On the geometry of two-dimensional slices of irregular level sets in turbulent flows. 2nd *Monte-Verita Colloquium on Fundamental Problematic Issues in Turbulence*, 22–28 March 1998 (Ascona, Switzerland), GALCIT Report FM98–2.

DIMOTAKIS, P. E., COOK, A. W., DEUSCH, S. B., PATTON, J. M. & LOMBEYDA, S. V. 1999 Rayleigh-Taylor Instability Studies from Direct Numerical Simulations. *Am. Phys. Soc.*, 52nd *Annual Meeting, Division of Fluid Dynamics*, (21–23 November 1999, New Orleans, LA), DN.01.

DIMOTAKIS, P. E., CATRAKIS, H. J. & FOURGUETTE, D. C. 1998 Beam Propagation and Phase-Front Integrals in High Reynolds Number Shear Layers and Jets. *AIAA* 29th *Plasmadynamics and Lasers Conference* (15–18 June 1998, Albuquerque, NM), Paper 98–2833.

DIMOTAKIS, P. E., CATRAKIS, H. J. & FOURGUETTE, D. C. 2001 Flow structure and optical beam propagation in high Reynolds number, gas-phase shear layers and jets. *J. Fluid Mech.* **433**, 105–134.

EGOLFOPOULOS, F. N. & DIMOTAKIS, P. E. 1998 Non-premixed hydrocarbon ignition at high strain rates. *Proc. Combustion Inst.* **27**, 641–648.

EGOLFOPOULOS, F. N. & DIMOTAKIS, P. E. 2000 Effects of additives on the non-premixed ignition of ethylene in air. *Combust. Sci. and Technol.* **156**, 173–199.

EGOLFOPOULOS, F. N. & DIMOTAKIS, P. E. 2000 A comparative study of ethylene kinetics in premixed and non-premixed flames. *Combust. Sci. and Technol.* (in press).

LAPPAS, T., LEONARD, A. & DIMOTAKIS, P. E. 1999 Riemann invariant manifolds for the multidimensional Euler equations. *SIAM J. Sci. Comp.* **20**(4), 1481–1512.

MEIRON, D. I., DIMOTAKIS, P. E. HENDERSON, R., KOSOVIC, B., PULLIN, D. I. & SAMTANEY, R. 2000 Direct numerical simulation and subgrid-scale modeling of

compressible turbulent mixing. 20th *IUTAM Congress*, 22 August – 2 September 2000 (Chicago, IL), Paper PC1.

PAPALEXANDRIS, M. V. 2000 A Numerical Study of Wedge-Induced Detonations. *Comb. and Flame* **120**, 526–538.

PITZ, R. W., WEHRMEYER, J. A., RIBAROV, L. A., OGUSS, D. A., BATLIWALA, F., DEBARBER, P. A., DEUSCH, S. & DIMOTAKIS, P. E. 2000 Unseeded Molecular Flow Tagging in Cold and Hot Flows Using Ozone and Hydroxyl Tagging Velocimetry. *Meas. Sc. & Tech.* **11**, 1259–1271.

SHAN, J. W. 2001 *Mixing and Isosurface Geometry in Turbulent Tranverse Jets.* California Institute of Technology, Ph.D. thesis.

SHAN, J. W. & DIMOTAKIS, P. E. 2000 Turbulent scalar mixing in transverse jets. *Am. Phys. Soc.*, 53nd *Annual Meeting, Division of Fluid Dynamics*, (19–21 November 2000, Washington, DC), Abstract BB.007.

SHAN, J. W. & DIMOTAKIS, P. E. 2001 Turbulent mixing in liquid-phase transverse jets. (in preparation).

SHAN, J. W., DIMOTAKIS, P. E. & LANG, D. B. 1999 Mixing and boundary-layer effects in turbulent transverse jets. *Am. Phys. Soc.*, 52nd *Annual Meeting, Division of Fluid Dynamics*, (21–23 November 1999, New Orleans, LA), GC.06.

SLESSOR, M. D. 1998 *Aspects of turbulent-shear-layer dynamics and mixing.* Ph.D. thesis, California Institute of Technology.

SLESSOR, M. D., BOND, C. L. & DIMOTAKIS, P. E. 1998 Turbulent shear-layer mixing at high Reynolds numbers: effects of inflow conditions. *J. Fluid Mech.* **376**, 115–138.

SLESSOR, M. D., ZHUANG, M. & DIMOTAKIS, P. E. 2000 Turbulent shear-layer mixing: growth-rate compressibility scaling. *J. Fluid Mech.* **414**, 35–45.

5. Collaborations, interactions, and transitions

Numerous interactions, participations and presentations at meetings, conferences, and seminars that took place during the three-year period of performance of this grant were summarized in the annual reports.

Progress and events not documented in the most-recent annual report (31 August 2000) that occurred prior to the end of the present Grant (30 November 2000) include:

- 29 August 2000: P. E. Dimotakis,"Recent advances in turbulent mixing," 20^{th} *IUTAM Congress*, 22 August – 2 September 2000 (Chicago, IL). Invited sectional lecture (Paper EW1).
- 11 September 2000: P. E. Dimotakis,"Progress in turbulent mixing." Invited lecture, Venderbilt U.
- 12 September 2000: P. E. Dimotakis, L. Ribarov, R. Pitz, S. Nandula, J. Wehrmeyer. Discussions on further collaboration on applications of Image Correlation Velocimetry to gas-phase, molecular-tagging techniques.
- 3 October 2000: J. Bergthorson, "An experimental investigation of C1-C2 hydrocarbon flames," GALCIT Fluid Mechanics Research Conference presentation.
- 3 October 2000: M. Wang, "Statistical and Spectral Analysis of High Schmidt Number Scalars in Grid Turbulence," GALCIT Fluid Mechanics Research Conference presentation.
- 20 October 2000: P. E. Dimotakis, "Fluid and Solid Mechanics," Workshop on *Barriers to Predictive Simulation in Science & Engineering*, Lawrence Livermore National Laboratory.
- 3 November 2000: P. E. Dimotakis, "Turbulent drag reduction," DARPA outbrief (Jason study).
- 7 November 2000: M. B. Johnson, "Mixing and Combustion in Complex High Speed Flows," GALCIT Fluid Mechanics Research Conference presentation.
- 19 November 2000: J. W. Shan and P. E. Dimotakis, "Turbulent scalar mixing in transverse jets," *Am. Phys. Soc.*, 53^{nd} *Annual Meeting, Division of Fluid Dynamics*, (19–21 November 2000, Washington, DC), BB.007.

Consultative and advisory functions to other labs, government agencies, especially AF and DoD (include institutions, locations, dates, names):

- Dimotakis, P. E.: Lawrence Livermore National Laboratories. Consulting on compressible turbulence and inertial-confinement fusion (1993 to present).
- Dimotakis, P. E.: JASON group, MITRE (1997 to present). Consulting to DARPA and other government agencies.

Transitions (cases where knowledge resulting from this research has, is, or will be used in a technology application):

- Contributions to High-Energy Laser (HEL) development (1970–90). Contact: Dr. Wilhelm Behrens (310 812–0468), TRW R1-1044, 1 Space Park, Redondo Beach, CA 90278.
  i. Shear-layer growth and entrainment data/models.
  ii. Reynolds-number effects on mixing.
  iii. Use of gas-mixtures for index-or-refraction matching.
  iv. Laser-induced fluorescence diagnostics.

New Discoveries, inventions, patents: None

6. Honors/awards

Honors, degrees, and awards received during period, as well as, 'lifetime achievement honors such as Nobel prize, honorary doctorates, and society fellowships prior to this effort:

- Bond, C. L.:
  - Ph.D., California Institute of Technology (June 1998).
- Dimotakis, P. E.:
  - John K. Northrop Chair, Aeronautics, Caltech (February 1995).
  - Associate Fellow, AIAA (June 1989).
  - Fellow, Am. Phys. Society (November 1980).

- Leonard, A.:
  - Fellow, Am. Phys. Society.
  - Vice-Chair, Am. Phys. Society, Division of Fluid Dynamics (1997).
  - Chair, Am. Phys. Society, Division of Fluid Dynamics (1998).
  - Theodore von Karman Chair, Aeronautics, Caltech (December 1999).
- Slessor, M. D.:
  - Ph.D., California Institute of Technology (June 1998).